Optical Materials: X 13 (2022) 100130

Contents lists available at ScienceDirect

Optical Materials: X

journal homepage: www.journals.elsevier.com/optical-materials-x

Planar microcavities: Materials and processing for light control

Heba Megahd, Davide Comoretto, Paola Lova *

Dipartimento di Chimica e Chimica Industriale, Università di Genova, Via Dodecaneso 31, 16146, Genova, Italy

ARTICLE INFO

Keywords:
microcavities
Microresonators
Refractive index
Distributed bragg reflectors
Optical confinement

ABSTRACT

Microcavities are a class of optical structures providing a versatile approach to engineering light matter interactions. In light of recent developments in materials processing technologies, in particular for organic and hybrid ones, and of the need for high efficiency optical systems, there has been extensive innovation and improvement in their design and realization leading to a multitude of structures and materials. Among these, closed multi-material microcavities or microresonators based on the effect of dielectric contrast have been attractive for their low losses, applicability in a wide spectral range, and customizability. High-dielectric contrast microcavities based on distributed Bragg reflectors have been adapted early on for their highly controlled fabrication and strong light confinement and proved to be essential in current technologies including lasers and light emitting diodes. In this review, we map their evolution from planar one-dimensional inorganic structures to more sophisticated designs incorporating various categories of organic and hybrid materials. Additionally, we provide an overview of state-of-the-art developments and limitations of this class of structures.

1. Introduction

Optical microcavities, also known as microresonators, are sub-micrometric structures capable of confining light in small volumes for a relatively long time. These structures have intrinsic natural resonance modes that can radically modify the local photonic density of states (LPDOS) and be designed by manipulating their component materials, dimensions and geometry [1,2]. As such, when coupled with opportune luminophores or light sources, microcavities have proven themselves valuable in a wide range of optical applications including filters [3], enhancing device efficiency [4], lasing [5], all-optical switching [6,7], optical detection [8], and chemical sensing down to single nanoparticles [9].

Very broadly, microcavities are commonly classified into three categories depending on the kind of structure used [1,2,10]. The first class is represented by whispering gallery resonators, where light is guided through total internal reflection along a "racetrack" of concave high refractive index material placed in a low refractive index material (e.g. air) as in microdiscs, microspheres, microrings (from top to bottom in Fig. 1a) [11]. This can be seen as analogous to the namesake effect in acoustics [12]. Conversely, the second and third types, which are based on standing electromagnetic waves, are photonic crystals and Fabry-Peròt cavities. Photonic crystal microcavities consist of a sub-micrometric ordered array of a repeating motif, where the symmetry of the crystal is broken by including a defect, usually containing an active material [13–17]. The crystal array is composed of materials with different refractive index arranged in a one-, two-, or three-dimensional lattice with pitch comparable to visible and near infrared wavelengths (from top to bottom in Fig. 1b) [18]. With respect to the latter, Fabry-Peròt cavities represent instead one of the more straightforward and widespread structures. In their simplest arrangement, these cavities consist of two reflective mirrors sandwiching the cavity layer (Fig. 1c). The mirrors can be metallic, dielectric or both, to form hybrid and plasmonic Fabry-Peròt cavities [19–21]. When metallic mirrors are employed, the relatively low reflectance and high absorbance of metals introduce losses limiting their performances and use [22]. Instead, employing one-dimensional planar photonic crystals, also known as dielectric mirrors or distributed Bragg reflectors (DBRs), provides ease of fabrication, high tunability and lower losses, which made them extensively researched. Indeed, there have been many comprehensive reviews and textbooks about the intricate physics of microcavities [2,11,23–25], coupling regimes [15,26,27], and their applications [28,29]. They have also been adopted into device designs such as vertical cavity surface emitting lasers (VCSELs), that have already been widely commercialized since the 1990s till this day [5], while pristine DBRs have been largely employed for a variety of technologically relevant applications [30] including sensing [31–35], light filtering [36], switching [37], and light harvesting enhancement in

* Corresponding author.
E-mail address: paola.lova@unige.it (P. Lova).

https://doi.org/10.1016/j.omx.2021.100130
Received 25 October 2021; Received in revised form 3 December 2021; Accepted 6 December 2021
Available online 28 December 2021

photovoltaic and photocatalytic systems [38,39].

The large interest in Fabry-Peròt cavities arose from the fact that while whispering gallery resonator and complex photonic structures provide high spatial and temporal confinement owing to large dielectric contrast and tri-dimensional confinement, their fabrication and design is neither simple nor straightforward. The spatial and temporal confinement of the electric field within the resonator are quantified by i) the mode volume (V_{eff}), which describes the effective volume where light is confined, related to the peak intensity of the electric field within the cavity (i.e., spatial confinement) and ii) the quality factor (Q), which relates to the rate of power loss inside the cavity, or the lifetime of photons in the cavity (i.e., temporal confinement) [40]. In non-planar systems the confinement is maximized as V_{eff} is small and Q is large owing to the high dielectric contrast obtained when coupling dielectrics or semiconductors with air as a low refractive index material, and to the three-dimensional confinements. Conversely, dielectric Fabry-Peròt microcavities consist of at least two different dielectric materials assembled into DBRs sandwiching a defect layer. On one side, the need for two materials reduces the dielectric contrast of the mirrors with respect to the other configurations, and on the other, it allows confinement only along the normal direction with respect to the lattice periodicity, thus affecting negatively V_{eff} and Q. Indeed, the planar configuration confines and enhances the intensity of the electric field, only along the normal direction with respect to the lattice periodicity, where the field penetrates the mirrors affecting the effective volume as will be described in section 3.1.

In detail, in these structures a standing electromagnetic wave with enhanced intensity is confined within a defect layer. For the longitudinal resonance mode (normal direction with respect to the plane), such wave consists of an integral number of half wavelengths of the length of the cavity mode. When an emitter is embedded in the defect layer, it can interact with the enhanced standing wave, whose enhancement depends on Q and V_{eff}, [2]. As larger field enhancement allows larger interactions, strategies to enhance light confinement -otherwise limited in planar systems- and thus to increase Q and decrease V_{eff}, are highly researched [1,26,41–47]. This review will focus on these strategies and will first introduce the basic working principles of dielectric mirror-based microcavities for emission control, and then target innovations in their design, fabrication and optimization, oriented towards performance enhancement. In addition, we will briefly address the figures of merit used to characterize confinement effects in these microcavities and how they are influenced by fabrication techniques and design.

2. Planar Fabry-Peròt dielectric cavity

Fig. 2a schematizes the structure of Fabry-Peròt dielectric cavity made of two DBRs separated by a defect layer. The planar DBRs constituting the mirrors are layered pairs of dielectric materials (bilayers) of relatively high and low refractive index (n_h, n_l) with respect to each other. Due to the consecutive refraction and reflection of light at the layer interfaces, a series of interference effects gives rise to wavelengths whose propagation is forbidden in the mirrors and are back-

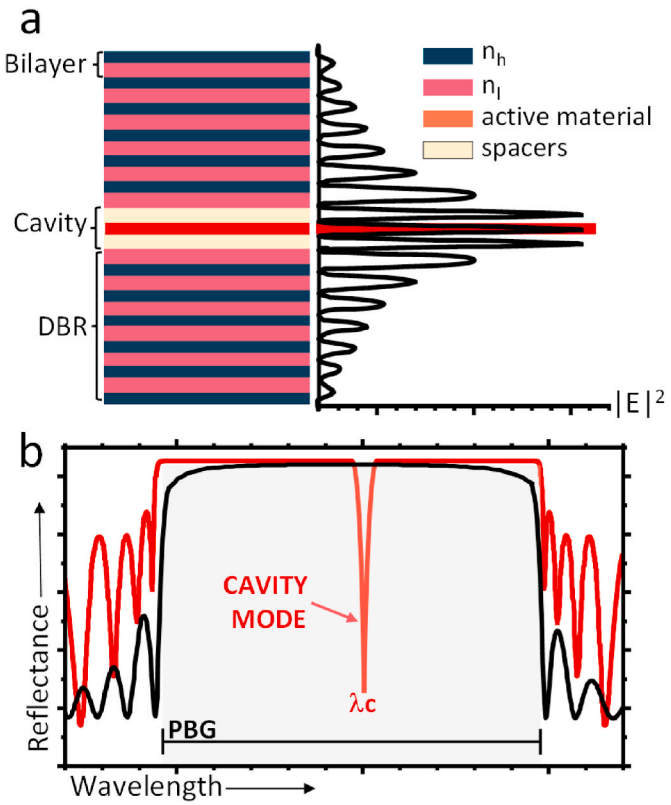

Fig. 2. (a) Schematic representation of planar microcavity and standing electromagnetic wave inside the cavity at λ_c; (b) Typical reflectance spectrum of DBR (black) and planar microcavity Red). (For interpretation of the references to color in this figure legend, the reader is referred to the Web version of this article.)

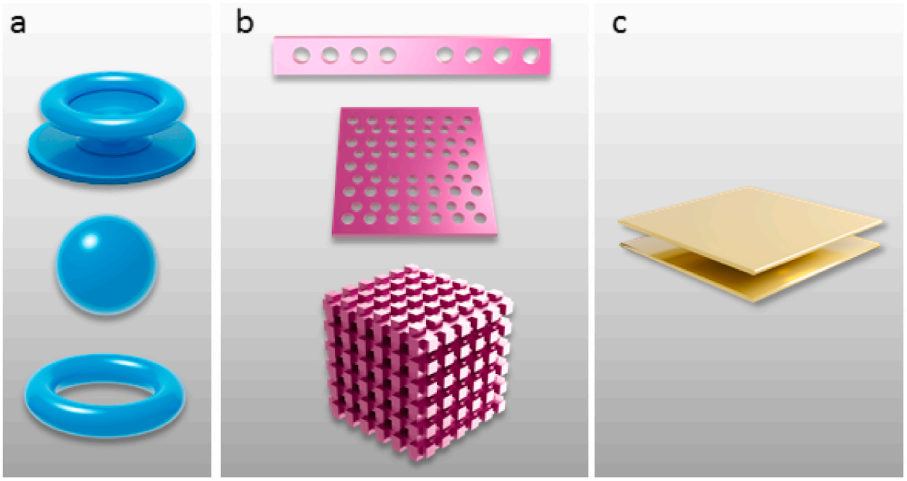

Fig. 1. Optical microcavity configurations. a) Whispering gallery mode designs: microdisk, microsphere and microring (from top to bottom); b) Photonic crystals: 1D, 2D, 3D (top to bottom); c) Fabry- Peròt cavity.

diffracted or reflected. These spectral regions are called the photonic band gaps (PBGs) [48]. As such, the reflectance spectrum of a DBR shows a highly reflecting peak assigned to the PBG (black line of Fig. 2b) due to the coherent diffraction of the light beam in the photonic crystal, together with a set of interference fringes which dominate the spectrum background that are due to the partial reflection at the first and last interfaces of the material, which in turn behaves as an effective medium [48]. In a manner analogous to diffraction, there can exist multiple PBG orders. In the λ/4 configuration, where the length of the layers of any ith material is $d_i = \frac{\lambda_{PBG}}{4n_i}$, the even orders are eliminated, and the intensity of the odd ones is maximized. Far from this condition, all diffracting orders are observed with different intensities depending on the ratio of the optical length of the different layers [49]. The peak reflectance at the PBG in this case can be approximated as a function of the refractive index of the materials used to construct the DBR and the number of bilayers (N) (Equation (1)) [29]. Therefore, it is possible to achieve very high reflectance with materials of high index contrast ($\Delta n = n_h - n_l$) using a relatively low number of bilayers, or vice versa.

$$R_{max} = \left[\frac{1 - n_s\left(\frac{n_l}{n_h}\right)^{2N}}{1 + n_s\left(\frac{n_l}{n_h}\right)^{2N}}\right]^2 \tag{1}$$

The refractive index also affects the width of the PBG, as in Equation (2) [49]:

$$\Delta E_{PBG} = \frac{4E_{PBG}}{\pi}\frac{n_h - n_l}{n_h + n_l} = \frac{4E_{PBG}}{\pi}\frac{\Delta n}{2n_h + \Delta n} \tag{2}$$

where ΔE_{PBG} and E_{PBG} are the width and position of the PBG in energy. The PBG spectral position can instead be easily designed as needed by modifying the lattice pitch (D) as described by the Bragg-Snell equation (Equation (3)), where m is the diffraction, or PBG, order, n_{eff} is the effective refractive index of the structure (Equation (4)) and θ is the angle of incidence of impinging light.

$$m\lambda_{PBG} = 2D\sqrt{n_{eff} - \sin^2\theta} \tag{3}$$

$$n_{eff} = \sqrt{\frac{d_1}{d_1 + d_2}(n_1)^2 + \frac{d_2}{d_1 + d_2}(n_2)^2} \tag{4}$$

In principle, the width and intensity of the PBG can be maximized employing air as low dielectric material [50–52], however, we do not consider such pairings in this review.

A defect layer in the lattice breaks the translational symmetry of the crystal, allowing the formation of a cavity mode, where light can propagate within the spectral domain of the PBG. These modes are detected as relative minima within the PBG in the reflectance spectrum of the structure (red line in Fig. 2b) [18]. These spectroscopic features can be described in terms of the changes in the LPDOS, which is deeply altered depending on the design of the cavity as will be discusses in section 3.

Fig. 2a shows a schematization of the electric field intensity along the normal direction in the microcavity structure. The field is characterized by an oscillation between maxima and minima that correspond to antinodes and nodes of the standing wave, respectively. The average intensity instead increases from the top and bottom surfaces to the center of the structure, where the cavity is placed. As a consequence, when the cavity is doped with a fluorophore, its emission can then be enhanced at the antinodes (maxima) or suppressed at the nodes (minima) of the standing wave. As a consequence, the geometrical placement superimposition between antinodes and emitter in the microcavity is essential to result in emission enhancement, and spacers are often used to control the position of the active material with regards to the electric field in the cavity [22,53]. To exploit these effects, the emission spectrum of the fluorophore must match the energy of the cavity mode. To this end, the optical properties of these structures, including reflectance and transmittance, can be simulated in a straightforward manner through transfer matrix method calculations [54], which provide a simple yet powerful tool to design the optical properties of the mirrors or planar cavities, which can be grown when suitable and accurate deposition techniques are employed. Consequently, the structure can be engineered to give rise to a high-transmission cavity mode that spectrally matches the fluorescence of a fluorophore embedded inside the cavity layer [2,11,13]. More sophisticated cavity designs can involve three mirrors with two defects, introducing multiple cavity modes in different spectral regions. This allows the coupling of emitters in different cavities to different cavity modes, creating multimode devices [55,56]. In general, the number of cavity modes, their wavelengths and their spacing depends on the optical thickness of the cavity layer [22]. The order of the cavity $m_c = Int\left(\frac{2nL_{MC}}{\lambda_c}\right)$ indicates the number of cavity modes, and since the cavity length (L_{MC}) is usually on the order of the wavelength of light, a low number of cavity modes exists within the PBG [22].

3. Light confinement effects in optical microcavities

As mentioned, the broken refractive index periodicity of planar microcavities deeply alters the LPDOS along the normal direction compared to free space (Fig. 3a). In a DBR the LPDOS is slightly enhanced at the two PBG edges and it goes to zero at the PBG (panel b) while, when a defect layer is present the density is dramatically enhanced at the cavity modes (panel c) [48]. The spectral variation of the LPDOS can affect strongly the emission properties of the fluorophore embedded into a cavity, giving rise to low values at the PBG wavelengths, and large ones at the cavity mode, intensifying the fluorescence signal at the cavity mode and inhibiting it at the PBG [22,57]. The different LPDOS can also modify the emission decay of the fluorophore compared to free-space, and the system can be described within Fermi's golden rule in the weak coupling regime. Importantly, the LPDOS, and then the effect of the structure on emission from planar microcavities have an angle-dependent and a polarization dependent behavior [22,57]. Moreover, no confinement is present along the parallel direction. Hence, this further highlights the importance of devising structures that extend the confinement into the three-dimensional realm and decrease the effective cavity volume.

The theoretical emission intensity enhancement at the cavity mode in the normal direction (G_e) can be estimated [58,59] from the reflectance of the top (R_1) and bottom (R_2) DBRs and the ratio between the emission lifetime in the cavity and that in free space $\frac{\tau_c^{rad}}{\tau_0^{rad}}$, while the ratio between the average square modulus of the electric field strength at the emitter position and at the maximum value in the cavity $\frac{|E|^2_{avg}}{|E|^2_{max}}$ reflects the positioning of the emitter with respect to the nodes and antinodes of the standing wave in the cavity (Equation (5)).

$$G_{e\ (th)} = \frac{|E|^2_{avg}}{|E|^2_{max}}\frac{\left(1 + \sqrt{R_2}\right)^2(1 - R_1)}{\left(1 - \sqrt{R_1 R_1}\right)^2}\frac{\tau_c^{rad}}{\tau_0^{rad}} \tag{5}$$

As such, intensity enhancement is often observed even without radiative rate variations [60–63]. However, the weak coupling between light and matter in the microcavity can also affect the rate of spontaneous emission from the cavity, which is the inverse of the radiative lifetime, in what is termed the Purcell effect. The Purcell factor (P) dictates the coupling strength, and consequently the extent of modification of radiative rate in cavity (Γ_c) for spontaneous emission with respect to emission in free space (Γ_0), depending on the cavity wavelength (λ_c), the refractive index of the cavity layer (n_c), and fundamentally on the ratio Q/V_{eff} (Equation (6)).

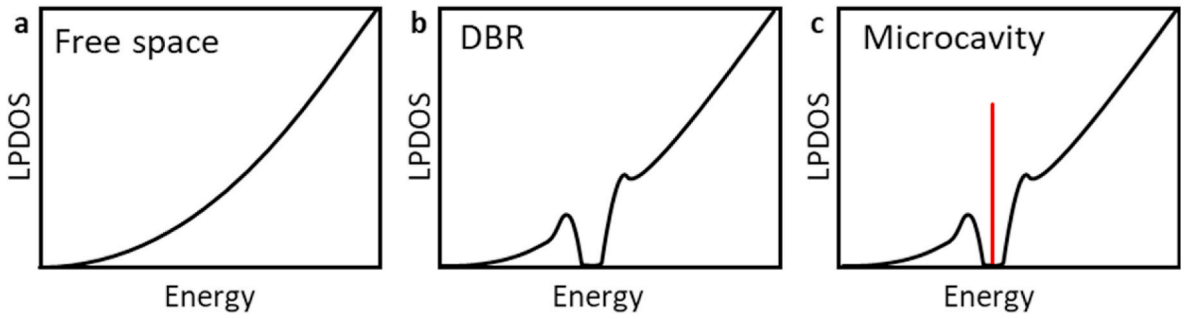

Fig. 3. LPDOS in free space (a); in a DBR (b); and in a planar microcavity (c).

$$P = \frac{\Gamma_c}{\Gamma_0} = \frac{\tau_0^{rad}}{\tau_c^{rad}} = \frac{3}{4\pi^2}\frac{\lambda_c^3}{n_c^3}\frac{Q}{V_{eff}} \tag{6}$$

For a luminescent material at λ_e with a linewidth smaller than the cavity mode $\Delta\lambda_c$, the emitter can be considered to couple to the cavity mode, altering the lifetime $\left(\tau = \frac{1}{\Gamma}\right)$ as inferred from Fermi's golden rule [64]. It should be noted that, as shown in Equation (7), other factors influence the radiative rate, including the positioning (r) of the emitter with respect to the antinodes of the cavity standing wave $(\frac{|E(r)|^2}{|E_{max}|^2})$ and the spectral mismatch between the cavity mode and the emission wavelength [2]. Factor *f*, on the other hand, represents the losses into the leaky modes that will be considered in the next section. This indicates that it is possible to achieve both radiative rate enhancement and suppression depending on the cavity design.

$$\frac{\tau_0}{\tau_c} = P\frac{2}{3}\frac{|E(r)|^2}{|E_{max}|^2}\frac{\Delta\lambda_C^2}{\Delta\lambda_C^2 + 4(\lambda_c - \lambda_e)^2} + f \tag{7}$$

High Purcell factors reflect a higher probability of amplified and spontaneous emission, which are essential for applications like low-threshold lasing [65] and low consumption light emitting devices [66]. It is also widely exploited to enhance light-matter interaction in single photon sources [67], and photovoltaic devices to increase device efficiency by reducing energy loss in unwanted radiative or nonradiative pathways [68]. As the Purcell factor is dependent on the ratio Q/V_{eff} (Eq. (6)), it is important to maximize the quality factor and minimize the effective volume in order to maximize the enhancement in the fluorophore radiative rate.

Moreover, enhancing the ratio between *Q* and V_{eff} can increase the exciton-photon coupling, moving from the weak to strong coupling regime [69] for a suitable emitter showing large fluorescence oscillator strength. In the case of the strong coupling regime, the cavity does not perturbate the radiative rate decay of the fluorophore while, the emitter and the cavity exchange energy at the Rabi frequency. Then, the coupling rate into the microcavity is faster than any loss mechanisms. This allows the formation of hybrid quasiparticles of photons and excitons, which enable the control of material properties, including chemical reaction rates and phase transitions [70]. As the coupling strength (or the Rabi frequency) is related to Refs. $1/\sqrt{V_{eff}}$ [71,72 and the loss rate is related to Q, the importance of simultaneously maximize *Q* and minimize V_{eff} is again evident [26,73]. In the next section, we address the physical meaning of both figures of merit and the role of the parameters affecting them.

3.1. Effective volume

The effective volume characterizes the geometrical light confinement within microcavities and can be calculated as a function of the relative permittivity $(\varepsilon(\vec{r}))$ and electric field describing the cavity mode $(E(\vec{r}))$ in the structure (Equation (8)) [2].

$$V_{eff} = \frac{\int \varepsilon(\vec{r})|E(\vec{r})|^2 dV}{\max\left(\varepsilon(\vec{r})|E(\vec{r})|^2\right)} \tag{8}$$

For dielectric cavities, the effective volume is limited by the refractive index of the medium. This provides a lower limit to the achievable spatial confinement to be as follows in the case of 3D confinement [47, 74] (Equation (9)).

$$V_{eff} \sim \left(\lambda_c/2n\right)^3 \tag{9}$$

In a one-dimensional cavity such as a planar microcavity, as the confinement is only in the normal dimension, the volume can be quantified in terms of the effective cavity length L_{eff} (Equation (10)) [75]. Then, this parameter can be expressed as a function of n_{eff} (Equation (4)). The effective length is inversely proportional to the refractive index contrast between the layers forming the DBRs. Therefore, higher dielectric contrast is important for reducing the effective length and achieving high confinement.

$$L_{eff} = L_{MC} + 2\,L_{DBR} \approx L_{MC} + 4(d_H + d_L)\frac{n_{eff}}{|n_H - n_L|} \tag{10}$$

3.2. Quality factor

The quality factor (*Q*) is instead a dimensionless parameter quantifying the rate loss as compared to the energy stored in the cavity. Therefore, a larger *Q* value indicates relatively low energy loss and longer confinement in the cavity [25]. In other words, it is defined as the number of optical cycles before damping to 1/e as in Equation (11), as the loss is exponential in nature [76]. As measured from the emission, transmission, or reflectance at the cavity mode (at wavelength λ_c and frequency ω_c), Q can be related to the linewidth full width at half maximum (FWHM, $\Delta\lambda$, $\Delta\omega$) of the cavity mode with respect to its spectral position.

$$Q = 2\pi\frac{stored\ energy}{power\ loss\ per\ round\ trip} = \frac{\lambda_c}{\Delta\lambda} = \frac{\omega_c}{\Delta\omega} \tag{11}$$

All the losses (γ) in a microcavity, regardless of their origin, are related to Q and determine the lifetime of photons in the cavity τ_c ($Q = 2\pi\nu_c\tau_c$), which in turn is related to the losses $\gamma = \tau_{tr}/\tau_c$ where τ_{tr} the transit time of photons in the cavity ($\tau_{tr} = n_{cav}l/c$). For DBR-based Fabry-Peròt cavities, *Q* can also be related to the effective microcavity mode order ($m_c = n + \frac{n_l}{\Delta n}$) [77] and the reflectivity (*R*) of the top and bottom DBRs (Equation (12)) [22,78], which depends on the refractive index of the materials employed in the DBRs (Equation (1)) [79].

$$Q = m_c\left[\frac{\pi(R_1R_2)^{\frac{1}{4}}}{1 - \sqrt{R_1R_2}}\right] \tag{12}$$

In this case, the effective mode order is introduced to account for the penetration of the field in the dielectric mirrors. It should be considered

that in a more realistic examination, loss mechanisms including material absorption, scattering, and coupling losses can increase the loss per round trip and hence deteriorate the quality factor of the microcavity [80,81], which then depends on fabrication methods and materials. Simply put, the actual quality factor Q_{act} (Equation (13)) is influenced by the intrinsic quality factor dictated by the ideal structure (Q_{int}), the extrinsic one representing inhomogeneities in the DBR and absorption losses (Q_{ext}), and that related to scattering Q_{scatt} [82].

$$\frac{1}{Q_{act}} = \frac{1}{Q_{int}} + \frac{1}{Q_{ext}} + \frac{1}{Q_{scatt}} \tag{13}$$

Eqs. (10) and (12) highlight the fundamental role of the dielectric contrast of the structures in both reducing the effective length and maximizing the quality factor of a microcavity.

4. Beyond one dimension

To reduce the effective volume in planar microcavities, it is possible either to embed 2D patterns in the cavity layer or to reduce the lateral dimension of the structure by etching. Embedding structures with different dimensionality within the planar cavity layer such as gratings [83], rings [67] and microspheres [84] can introduce efficiently lateral confinement in the structure. On the other hand, refractive index mismatch at the interface of the inserted structures can cause scattering and refraction losses [85]. In addition, more exotic structures such as open cavities employing curved DBRs [86], optomechanical systems [87], or hybrid metallo-dielectric cavities [19,20] have also been investigated. A more viable approach, which is currently limited to inorganic materials [88–90], consists in reducing the lateral dimension of the DBR by etching micropillars in the planar structure. In this manner, the dielectric contrast between the high-index inorganic materials and the surrounding air leads to reflection at the lateral interface, and thus, three-dimensional confinement [81,91]. Compared to 3D photonic crystals, in micropillars the narrow escape cone in efficient Gaussian-like pattern in the normal direction makes the extraction of light more efficient for applications that need directional emission or efficient single photon sources due to the low beam divergence [92,93]. Fig. 4 schematizes some micropillar designs and geometries reported in literature to further improve confinement.

Cylindrical micropillars with diameters of 2–5 μm (Fig. 4a) are commonly etched by focused ion beam. Decreasing their diameter below 2 μm also decreases dramatically the quality factor [94], which is regularly lower than for un-etched planar microcavities [95] owing to the introduction of fabrication artifacts such as corrugation and oxides deposit cladding during the etching [92]. Nonetheless, the decrease in V_{eff} more than compensates for this effect. Thus, Purcell factors larger than 30 can be reached [93], which is an order of magnitude larger than for un-patterned planar structures [96]. Regarding the geometry, circular cross sections are by far the most common, while more complex geometries can lead to unusual effects. For example, in microcavities with an elliptical cross section, breaking the symmetry of the pillars lifts the polarization degeneracy and give rise to polarized response both in experimental and theoretical investigations [97]. Polygonal cavities are not so popular, however some experimental and theoretical studies hypothesize that they also have strong chirality [98]. Laser micromachined confinement system used to produce waveguides and sensors could be also a tool for future developments [99,100].

Going back to circular cross-section microcavities, introducing a smoother transition between the DBRs and the cavity layer through insertion of additional DBR structures [101,102] can lead to large quality factors even for submicrometric diameters [103,104]. For this structures, termed tapered or adiabatic micropillars (Fig. 4 b), Zhang et al. deposited additional DBRs between the main mirrors and the active layer. These “taper” or adiabatic pairs maintain the thickness ratio of the main DBRs but have a smaller periodicity, which reduces scattering losses due to the difference between the cavity mode and the penetrating mode in the dielectric mirrors. Both experimental data and models support the significant increase in Q up to 3×10^6, and decrease of V_{eff} down to $0.1\lambda/n^3$ with ten taper segments, enhancing Q/V_{eff} by more than 3 orders of magnitude compared to conventional designs [103].

Needless to say, while reflectance of DBRs is commonly larger than 99%, the reflectance of the etched cavity sidewall is much smaller and approaches, for instance, 31% for GaAs-based micropillars, and much lower values for materials with lower dielectric contrast with air, including polymers [105]. This leads to the persistence of “leaky modes” where photons with energy comparable to the PBG are guided into. This hinder off-resonance coupling to the cavity mode and strong inhibition of fluorescence in the micropillars, which then behave similarly to unetched planar cavities [107]. However, coating the pillars with metals, such as gold, enables radiative rate decrease of 50% [107]. The work by Gérard et al. has solidified the importance of controlling and accounting for the leaky modes when considering the Purcell effect in microcavities [107]. By coating micropillar sidewalls with gold, they demonstrated that high radiative rate suppression in micropillars is possible by suppressing coupling to leaky modes (Equation (7)). Again, the high loss of metals has prompted Jakubczyk et al. to encapsulate the dielectric micropillars in a radially distributed dielectric mirror cast through oblique incidence pulsed laser deposition (Fig. 4 c), thus providing high reflectivity and low losses also in the lateral direction. The additional radial confinement can introduce further scattering losses (Equation (13)) that can be avoided through engineering the micropillar modes using tapering [105].

Finally, one very interesting configuration for micropillars was

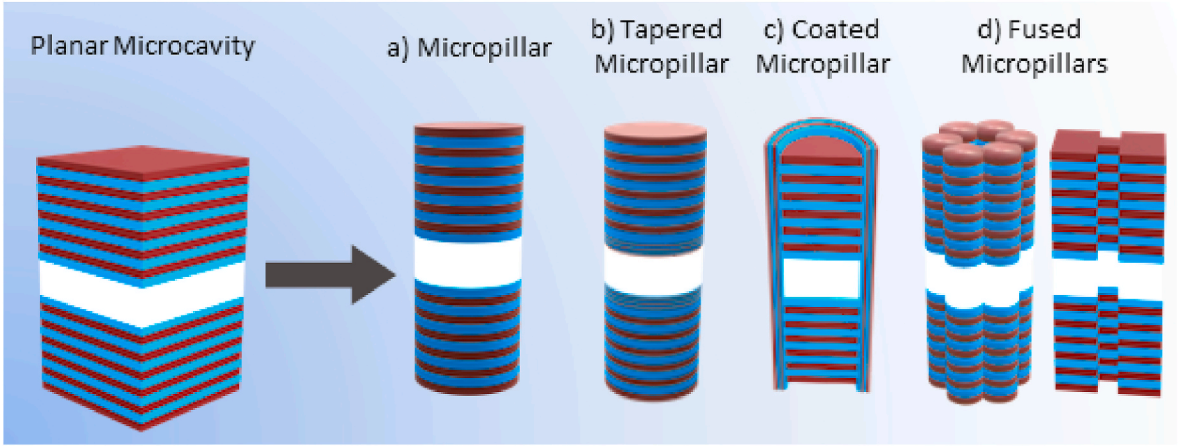

Fig. 4. Different micropillar configurations: (a) Simple micropillar; (b) Tapered micropillar [103]; (c) Coated micropillar [105]; (d) Fused micropillars [98,106].

motivated by creating complex optical modes in the cavities. Fig. 4 d shows two examples of fused micropillars, based on circular or square cross-sectioned pillars connected together. Since in an individual pillar light is confined in three dimensions creating discrete optical modes for photons, it can be seen as analogous to electronic states in an atom. Starting with the work of Baye [98], the creation of fused cavities creates coupled optical modes, similar to electronic modes in molecules, hence their name "optical molecules" [97,108,109]. In such configurations, there exists coupling of modes, energy discretization in "energy levels" as well as chirality [106]. The coupled pillars can have different diameters that allow photon transfer, achieving localized and delocalized resonator modes [110]. These types of configurations can form a basis for the interaction of spatially separated quantum dots and realization of entangled photons generated by two quantum dots [98]. Very recently, arrays of fused hexagon micropillar topological insulators have been shown to act as coherent laser sources [111].

5. Nanofabrication and materials limitations

The range of materials available for the fabrication of DBRs and microcavities is dictated by the need for wide transparency in the ultraviolet to the near-infrared window, depending on the application. In addition, it is limited by the availability of fabrication processes capable of high dimensionality control as well as high thickness homogeneity, low scattering, and possible pairing of materials in multi-layered structures.

Since the beginning of research into quantum cavity electrodynamics using DBRs, inorganic materials have been at the forefront of research [112] thanks to the wide variety of materials providing large dielectric contrast and to the multitude of compatible thin-layer fabrication techniques [113]. Table 1 summarizes the techniques commonly employed in literature along with the materials that can be processed. Among them. Epitaxy techniques provide incredibly low roughness of the order of a few atomic layers [77], making them an extremely controllable route to fabricating microcavities. In addition, the optical properties can be monitored during the growth process for in situ quality control [114]. This has made epitaxy techniques the most widely used for fabricating semiconductor microcavities. However, they require high temperature, high or ultrahigh vacuum and their high thickness control comes at the cost of slow deposition rates and high costs. Chemical and physical vapor deposition methods require less extreme fabrication conditions, provide acceptable dimensional control and can be used for a wide range of materials, including both inorganics [112] and polymers [115]. Indeed, some vapor deposition methods allow holding the substrate at room temperature, allowing the combination of inorganic mirrors with organic emitters [116]. However, the easiest and most cost effective deposition techniques are those based on solution-processing which does not require high temperature or vacuum and can be used for growing polymeric, inorganic or hybrid DBR starting from polymer solutions, sol-gel precursors or particle suspensions. In that case, layers can be deposited on a substrate by spin coating, where solutions/suspensions are deposited on a rotating substrate, or by dipping the substrate in a solution or a colloidal suspension [49]. Alternating repeated deposition processes allow the growth of DBRs and microcavities with sub-nanometer scale layer thickness control. However, in the case of polymers, solution processing limits the possible materials to those soluble in orthogonal solvents. In addition, solution processing often compromises the interface quality, which is lower than the previously mentioned evaporation techniques, especially in the case of inorganics utilizing colloidal suspensions [49,117], while for polymer systems it is sub-nanometric [49].

Table 1
Thin-film deposition processes and materials used to fabricate DBRs.

Process		Example of materials
Epitaxy	Molecular beam epitaxy (MBE) Mask molecular beam epitaxy Organometallic vapor phase epitaxy	Semiconductor single crystals [58, 118–120], superlattices [97,121]
Physical Vapor Deposition	Thermal evaporation Electron-beam evaporation Plasma-assisted evaporation Sputtering Radio-frequency magnetron sputtering Oblique incidence pulsed laser deposition (OIPLD)	Oxides, nitrides, fluorides [116, 122–125]
Chemical Vapor Deposition	Reactive sublimation Plasma-enhanced chemical vapor deposition	Oxides, nitrides, semiconductors [116,126,127]
Hybrid Methods	Reactive helicon-wave-excited-plasma sputtering	Oxides [128]
Solution-Processing	Spin coating Dip-coating	Oxide nanoparticle and sol-gel processes [129], polymers [60, 130–132]

Regarding materials, semiconductors have been extensively used for the fabrication of DBR-based microcavities. This comes as no surprise due to the historical development of thin-film deposition techniques for electronic device fabrication [113]. The most used pairings include AlAs with $Al_xGa_{1-x}As$ [77], AlAs and GaAs [58,94,119] as well as $Al_xGa_{1-x}As$ [118,133] with different Al fractions and doping to control the refractive index [134]. Using epitaxial growth techniques, it is possible to control monolayer-deposition, providing extremely accurate thickness and positioning control as they have similar lattice parameters and high dielectric contrast. The high technological advancement in these types of materials has led them to be adopted early on for optoelectronic devices [135]. Pairing zinc-based semiconductors like zinc telluride and their superlattices including (ZnTe|MgSe|ZnTe|MgTe) [136] is not uncommon, due to the possibility of lattice-parameter matching during epitaxial growth [97,121]. However, it is impractical to use semiconductors due to their high absorption. To this end, oxide-based glasses are some of the most commonly used materials due to their broad band transparency and good mechanical and environmental resistance [137]. Among them, silicon dioxide is widely employed as low index medium due to its high transparency in the visible and NIR spectral ranges, ease of deposition and wide establishment of protocols for silica thin-film fabrication. Moreover, it is possible to use silica as both the high and low index materials by controlling its porosity, and consequently the effective refractive index of the layer [138,139]. In the infrared range, silica can also be coupled with silicon [140], whose application is, on the other hand, limited in the UV–Vis due to high absorption. The most commonly paired material with silica as a high index material is titania [123,141–143]. From the 1990s to now, the high dielectric contrast between the two materials (0.698 at 550 nm, see Fig. 5) and fabrication techniques useable for both materials has made them highly employed at industrial level. Radiofrequency sputtering [125,144], spin-coating [61], and e-beam evaporation [83,123,145] are some of the techniques used to fabricate SiO_2/TiO_2 microcavities, which provide a wide range of fabrication conditions, also allowing the cavities to include either inorganic or organic fluorophores. The choice of the material pairs does not only depend on the achievable contrast, but also the suitability of the fabrication technique and their long-time open-air stability, which makes silica and titania also highly commercially viable. However, nitrides and sulfides like Si_3N_4 and ZnS have been also used with silica [146,147]. Another high index oxide commonly paired with silica in research is tantalum pentoxide (Ta_2O_5) [148–151] which is colorless and has relatively low absorption in the visible and NIR. Like titania, it is possible to fabricate thin films of Ta_2O_5 through solution based sol-gel methods [151]. Other high-index metal oxides used in tandem with silica include HfO_2 [122], Nb_2O_5 [152] and ZrO_2 [128]. The latter is also used in a yttria-stabilized form (Yttria-stabilized zirconia, YSZ) [105]. In that case, it was reportedly paired with alumina for

the formation of radial DBRs. Paired with lithium fluoride, tellurium dioxide was also used as a high-index material [4,124]. Lately, more investigations are performed to expand the range of materials for more specialized practical applications [79,112]. For example, the desire to integrate planar microcavities within light emitting diodes (LEDs) to enhance their efficiency has been a motivation to develop conducting, metal-free DBRs, like those developed by Puzzo et al. using antimony-doped tin oxide (ATO) and tin-doped indium oxide (ITO) [153], where ATO was deposited via sol-gel processes and ITO was through sputtering. ITO has been deposited in multilayered structures also from nanoparticles dispersion [154]. In order to develop devices with broadband tunable emission, there is an interest also in integrating electrochromic DBRs in light emitting devices or lasers. For example, Xiao et al. reported on the electromodulation of luminescence wavelength, intensity, and quality factor from a microcavity by using WO_3 as the building block of the DBRs. In this case, applying voltage changes the absorption and refractive index of the material, which was used both as low index and high index material through varying the porosity, leading to control of emission from quantum dots [155].

Generally, while inorganic materials are excellent in terms of optical properties including transparency and refractive index variety, they are fragile and not flexible. Moreover, widely used vacuum and ultra-high vacuum deposition techniques poses some constraints to large area fabrication. Despite having high stability as individual thin films, the hybrid nature of the microcavity structure can result in graining, delamination and cracking due to the mismatch of their intrinsic mechanical properties. In addition, some are highly absorbing the visible region, limiting their application to the far-infrared [156]. To overcome these limits, in the last two decades a large effort has been put to developing structure with polymer dielectric materials that are easy to process, transparent in the visible region, and can be loaded with a wide range of other organic and inorganic materials. Besides, they display high mechanical flexibility, can be used as free-standing films and can be fabricated on a large scale [49]. However, their relatively easy fabrication through solution processing methods like spin-coating comes at the cost of limiting the pairs of mutually processable materials and their refractive index contrast [49]. Therefore, the relatively low dielectric contrast of transparent polymers compared to inorganics limits field confinement, and thus emission enhancement in microcavities. Lately, photonic structures involving the use of polymer materials have been a subject of increasing research [48,157]. Recently, Lova et al. have provided a detailed description of the challenges and advantages of using solution-processes polymers and polymer-inorganic composites in planar DBRs [79]. There have been significant advancements in developing polymer DBRs that provide a dielectric contrast comparable to their inorganic counterparts. For example, high refractive index polymers, with conjugated backbones and a high density of delocalized electrons are interesting for applications in the NIR spectral region. On the other hand, high absorbance in the visible spectral range limits their use [49]. Then, polymers with non-conjugated backbones and relatively small conjugated ramification such as poly (*N*- vinylcarbazole) (PVK) are often used as a high-index material in all-polymer dielectric mirrors [40,49,132,158] due to transparency in the visible spectral range, excellent processability and relatively high refractive index (see Table 2). On the other hand, high-index polymers with backbones containing polarizable atoms [159] such as polyimides and thio-derivatives [160–163], certain highly halogenated polymers [164] and systems containing phosphor [165–167] or hyperbranched polymers [168–170] have been used to fabricate DBRs, but have not been investigated in microcavities. Conversely, very low refractive indexes can be obtained by inserting voids and porosity in the polymer thin layers [159,171–176] or through using low index perfluorinated polymers, showing refractive indexes as low as 1.33 [172,177–180]. However, their low wettability and chemical stability necessitates surface activation to enable adhesion to other layers and have also not been explored for use in microcavities. As a result of the recent work in the field, polymer-based microcavities demonstrated high intensity enhancement from fluorophores, as well as emission lifetime change [132,181–183]. Nonetheless, the lower dielectric contrast compared to inorganic pairs necessitates the use of a greater number of bilayers to achieve higher reflectance as discussed in section 2. This results in a larger probability of introducing defects within the structure, which might be responsible to further reduce the quality factors reported for all-polymer systems so far as compared to their inorganic counterparts.

Fig. 5 depicts the dielectric contrast at 550 nm for some of the most reported material pairings. As the refractive index depends also on the processing conditions, we considered the value for non-porous and

Table 2
Tabulated refractive index for some bulk materials used as DBR components in microcavities. Actual values may differ based on the deposition or growth method.

	Material	UV (350 nm)	Vis (550 nm)	NIR (1500 nm)	Ref.
Inorganic	**AlAs**	4.3848	3.199	2.8950	[184, 185]
	GaAs	3.4623	4.0049	3.3608	[186]
	$Al_xGa_{x-1}As$ (19.8% Al)	3.6397	3.9093	3.4570	[186]
	Al_2O_3	1.7972	1.7704	1.7470	[187]
	ZnS	2.7957	2.3858	2.2792	[188, 189]
	ZnTe	4.1313	3.2647	2.7355	[190, 191]
	ZnSe	2.9249	2.6520	2.4496	[191, 192]
	SiO_2	1.4820	1.4661	1.4575	[193]
	SiN	2.0040	1.9170	1.8770	[194]
	Si_3N_4	2.1339	2.0523	1.9977	[195]
	TiO_2	2.5853	2.1644	2.0576	[196]
	Ta_2O_5	2.2571	2.1157	2.0589	[193, 197]
	Nb_2O_5	2.7622	2.3603	2.2370	[198]
	TeO_2	2.4412 (@ 400 nm)	2.2913	2.2079 (@1 mm)	[199]
	ZrO_2	2.2536	2.1661	2.1103	[200]
	CaF	1.4465	1.4348	1.4263	[201]
	LiF	1.4028	1.3930	1.3832	[202]
	HfO_2	1.9649	1.9021	1.8779	[203]
	YSZ	2.2536	2.1661	2.1113	[200]
Polymers	**PS**	1.6536	1.5934	1.5646	[204]
	CA	1.5092	1.4774	1.4605	[48]
	PAA	1.5399	1.5187	1.5081	[60]
	PVK	1.8995	1.692	1.6775	[205]

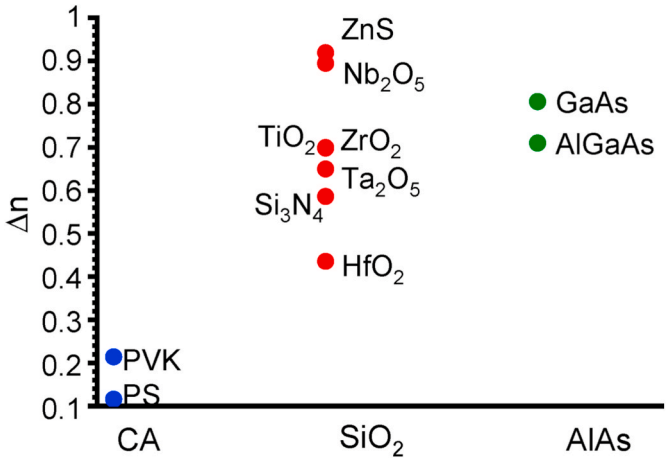

Fig. 5. Comparison between refractive index contrast at 550 nm for commonly used high index materials paired with the typical low index one used for the growth of DBRs. For polymers, cellulose acetate; for insulators, SiO_2; for semiconductor AlAs.

undoped materials as reported in literature (see Table 2). There, the x-scale shows the low refractive index materials, while the y-axis shows the contrast value obtained pairing the latter with different mutually processable high index materials. For polymers, cellulose acetate (CA, n = 1.46) has been widely reported paired to polystyrene (PS, n = 1.58) and PVK (n = 1.68). These polymer-polymer pairs provide a significantly lower contrast compared to their organic counterparts (0.11–0.21). However, better performance low-index polymers such as perfluorinated ones (n = 1.33–1.35) can result in higher refractive index contrast as stated earlier [79]. When silica is employed as low index material (n = 1.46), the contrast can exceed 0.9, even excluding the pairing with silicon, which can reach 2.9. The figures given for semiconductor pairings including AlAs and GaAs or $Al_xGa_{1-x}As$ are only indicative, as they do not consider refractive index changes and tuning by doping the crystalline structure, however, values easily exceed 0.8. Table 2 gives a wider picture of the refractive index of the commonly used materials to construct DBRs, reporting their refractive index in the near UV, visible and the NIR. It is important to highlight that the effective refractive indices of the materials and, consequently, the achieved contrast depend highly on the method and parameters used for the fabrication of the structure and the resulting porosity [206,207]. Hence, the values of the refractive index reported in the table are for dense materials as disclosed in the respective references.

The data are also summarized in Table 3, where the most common polymers and inorganic pairings are reported together with the relative index contrast values at the microcavity wavelength. For all-polymer microcavities employing PVK as a high index material and CA as a low index material, the cavity modes were tuned in the green-red range (564–657). The reported refractive index contrast approaches 0.2–0.22, consistent with the small dispersion on the refractive index of these materials in the wavelength range of interest. Regarding oxides, SiO_2/TiO_2 is the most reported pairing. These materials are often used for the spectral window just mentioned, where the contrast is reported between 0.76 and 1.01, at least 3.45 times larger than for polymer pairs. The wide range of contrast values can be attributed to the variation of the effective indices of the oxides depending on their fabrication method as well as to their spectral dispersion, as discussed earlier. Last, the contrast reached using semiconductor pairs such as AlAs-GaAs is comparable to that achievable with inorganic oxides. However, due to their absorbances in the visible range, they are more commonly used in the near infrared spectral range.

Polymer-inorganic nanocomposites promises to bridge the gap between the ease of processability of polymers and the high index of inorganics when high inorganic loads [180,214–216] are employed in polymer matrices [174,180]. In this case polymers act as binder for metal-oxides [217–222] and organometallics [223–225] nanoparticles displaying effective refractive index as high as 1.94 and high transparency in the visible spectral range [180,226,227]. These were paired with hyperbranched or fluorinated polymers as low-index materials, achieving a dielectric contrast in the range of 0.55–0.57 [180]. Several inorganic fillers have been used for the fabrication of DBRs, including TiO_2 [228,229], SiO_2 [230], ZnO [214,231,232], ZrO [233], and metal nanoparticles [115,234]. However, these are yet to be explored as building blocks in microcavities. Furthermore, polymers are also interesting as emitters [116]. The excitonic properties of organic emitters, including conjugated polymers, that will be further discussed in section 6, allow indeed to observe room-temperature strong-coupling effects in inorganic microcavities [235]. In the simplest case, the emitters can be spin-cast on the bottom DBR, and then the top DBR can be mechanically transferred on top to complete the cavity [124]. While this avoids exposing the polymer to high vacuum or temperature, the poor control of the mechanical transfer results in low quality of the microcavity. More favorably, using low-temperature vacuum techniques allows the direct deposition of the inorganic DBRs on top of the organic emitter with little to no degradation [116,123,138,146,236,237].

Table 3
Reported values for refractive index in planar microcavities employing the most common pairings.

Materials Pairing	Reported Refractive Index Contrast	Cavity Wavelength (nm)
CA-PVK	0.21 [181]	580
	0.21 [208]	657
	0.20 [40]	527
	0.22 [183]	564
SiO_2-TiO_2	0.95 [4]	545,560,580
	0.80 [117]	519
	1.01 [209]	607
	0.76 [125]	515
	0.89 [210]	514
	0.90 [103]	637
AlAs-GaAs	0.57 [211]	972
	0.60 [212]	919
	0.49 [213]	1491.6,1516.2

Regarding quality factors, values on the order of hundreds are routinely achieved in both inorganic and organic microcavities. However, scattering and roughness can cause lower quality factors of 30–85 in some inorganic ones [152,153]. On the other hand, highly controlled semiconductor cavities fabricated through processes such as molecular beam epitaxy typically have quality factors on the order of 10^3-10^4 in their planar configuration. The effect of the processing condition can be evaluated from SiO_2/TiO_2 microcavities fabricated through different methods. For example, for cavities fabricated through sol-gel processes, a quality factor of 250 was achieved [238], compared to values about an order of magnitude higher obtained through e-beam evaporation [129]. As such, the choice of materials does not only influence Q and V_{eff} through the control of the refractive index contrast that, as mentioned, also depends on deposition method, but also through the quality of the microcavity interfaces allowed through the different fabrication techniques. Regarding micropillars instead, disorder and inhomogeneity introduced at the sidewalls can significantly decrease the quality factor [92], even though very large values approaching 10^4 can be obtained [94]. This has been attributed to the higher number of bilayers used in the mirrors and the optimal quality of the pillar sidewalls due to the use of electron cyclotron resonance to enhance the reactive ion etching process. In the case of microcavities consisting in inorganic mirrors and an organic cavity layer, quality factors over 2100 have been measured [116]. The choice between organic or inorganic emitters in the cavity layer brings us to a comparison of the various emitters types that have been used to study microcavities.

6. Emitters and gain materials

A large array of materials are available for integration with microcavities, and choosing the appropriate pairing of emitters and photonic structures is an important part of cavity design [239]. Fundamental characteristics such as excitation wavelength, photoluminescence or electroluminescence wavelength and emission FWHM are important for the engineering the optical properties of the microcavity to enable the appropriate pumping of the fluorophore while tuning the cavity mode to achieve enhancement and inhibition of emission as desired. Narrow emitters are preferred for application investigating cavity quantum electrodynamics and both the weak and strong coupling regimes. To this end, the integration of rare earth ions like Er^{3+} has been achieved easily through ion implantation in microcavity layers [137]. Thus, they were used since the 1990s to study microcavity effects, especially in the NIR range. Both radiative rate enhancement and inhibition have been observed in inorganic planar cavities containing Er^{3+} [140].

The possibility of placing emitters at specific positions relative to the confined electromagnetic standing wave is fundamental in controlling rate enhancement as previously discussed in section 3.1 (Equation (8)). Inorganic quantum-confined emitters such as quantum wells of InGaN [240], GaAs [241], Zn-Cd-Se [242] and $In_xGa_{1-x}As$ [243] and quantum dots [244] provide excellent placement control, confinement, and

narrow emission. Through using epitaxial growth techniques, it is possible to place quantum wells at the antinodes of the standing wave inside the cavity [245]. In the case of quantum dots, they are easy to introduce into planar cavities [246] or micropillars [120], even using solution processing [209]. Their emission can also be easily tuned with temperature control, they do not undergo photobleaching, and are available at many emission wavelengths by compositional tuning that can be combined to engineer a specific overall spectral output [247]. In addition, they can be used to fabricate single-photon emission in micropillars, where single dots in pillars can be isolated as to investigate only one dot per pillar [248]. Recently, perovskites have attracted attention as emitters and gain materials in microcavities due to their long carrier lifetime, high photoluminescence quantum yield and high gain [249]. When perovskite quantum dots are used they usually need to be embedded in a matrix of another material for ease of processing and stabilization. In case of dispersing an emitter in a matrix, it is also important to match the refractive index between the embedded emitter and matrix to minimize scattering at their interface and obtain films of high optical quality [250]. Intensity enhancement while maintaining high quantum yield, Purcell enhancement [250], and strong coupling [251] have been observed for perovskites in microcavities. Thin crystals and 2D materials such as atomically thin transition metal dichalcogenide crystals (TMDCs) [252] such as MoS_2 are gaining popularity as emitters due to their very high exciton binding energies, and anisotropic properties [253]. More cutting-edge emitters such as trapped single atoms and vacancy centers in diamond nanocrystals [254] have been embedded in microcavities for studying quantum cavity electrodynamics in both weak and strong coupling regimes [255].

On the other hand, organic emitters provide excitons with high oscillator strengths at room temperature, high fluorescence quantum yield and can be easily processed into thin films, making them widely studied as emitters in microcavities. Their broad spectral width due to vibronic sidebands and strong inhomogeneous broadening of their electronic transitions makes their integration in microcavities preferential to achieve high color purity. Organic fluorophores such as porphyrin [256,257], molecular dyes [237], conjugated polymers [150,151,258], J-aggregates [60,259], and oligomers [260–262] have been integrated within both organic and inorganic cavities [237].

7. Conclusion and perspective

This review has highlighted the features and characteristics of planar microcavities based on dielectric mirrors. We reported on the role of the optimization of microcavities' figures of merit and on their relation to dielectric contrast among the composing materials. To increase the confinement effects, different micropillar designs can be etched from planar ones to observe three-dimensional confinement, this also allows enhancing the coupling between emitters and the cavity mode by suppressing leaky modes. A thorough review of the literature allowed showcasing frequently used materials for fabricating dielectric mirrors, whether organic or inorganic, which offer distinctly different refractive index contrast. While both the quality factor and the effective volume are affected by cavity design and materials, they are also influenced by the optical quality of the cavities and the fabrication techniques. We have shown that more controlled fabrication techniques offer higher microcavity qualities, however, a compromise is needed for considerations of cost, scalability, and ease of fabrication. In summary, there continues to be great developments in the field of dielectric mirror-based microcavities and further development is needed to advance the field.

CRediT authorship contribution statement

Heba Megahd: Data curation, Writing – original draft, Writing – review & editing. **Davide Comoretto:** Funding acquisition, Supervision, Writing – review & editing. **Paola Lova:** Conceptualization, Funding acquisition, Supervision, Writing – review & editing.

Declaration of competing interest

The authors declare that they have no known competing financial interests or personal relationships that could have appeared to influence the work reported in this paper.

Acknowledgments

This work was supported by the University of Genova [FRA 2019 and FRA 2020]

References

[1] K.J. Vahala, Optical microcavities, Nature 424 (2003) 839–846.
[2] A. Kavokin, J.J. Baumberg, G. Malpuech, F.P. Laussy, Microcavities, Second Ed, Oxford University Press, Oxford, 2017.
[3] F. Monifi, Ş.K. Özdemir, L. Yang, Tunable add-drop filter using an active whispering gallery mode microcavity, Appl. Phys. Lett. 103 (2013) 181103.
[4] R.H. Jordan, A. Dodabalapur, R.E. Slusher, Efficiency enhancement of microcavity organic light emitting diodes, Appl. Phys. Lett. 69 (1996) 1997–1999.
[5] R. Michalzik, VCSEL fundamentals, in: R. Michalzik (Ed.), VCSELs: Fundamentals, Technology and Applications of Vertical-Cavity Surface-Emitting Lasers, Springer Berlin Heidelberg, Berlin, Heidelberg, 2013, pp. 19–75.
[6] H. Nakamura, Y. Sugimoto, K. Kanamoto, N. Ikeda, Y. Tanaka, Y. Nakamura, S. Ohkouchi, Y. Watanabe, K. Inoue, H. Ishikawa, K. Asakawa, Ultra-fast photonic crystal/quantum dot all-optical switch for future photonic networks, Opt. Express 12 (2004) 6606–6614.
[7] G. Ma, J. Shen, Z. Zhang, Z. Hua, S.H. Tang, Ultrafast all-optical switching in one-dimensional photonic crystal with two defects, Opt. Express 14 (2006) 858–865.
[8] M. Furchi, A. Urich, A. Pospischil, G. Lilley, K. Unterrainer, H. Detz, P. Klang, A. M. Andrews, W. Schrenk, G. Strasser, T. Mueller, Microcavity-integrated graphene photodetector, Nano Lett. 12 (2012) 2773–2777.
[9] Y. Zhi, X.-C. Yu, Q. Gong, L. Yang, Y.-F. Xiao, Single nanoparticle detection using optical microcavities, Adv. Mater 29 (2017) 1604920.
[10] S. Cundiff, M. Kira, Semiconductor Quantum Science and Technology, Academic Press, Cambridge, MA, 2020.
[11] K. Vahala, Optical Microcavities, World Scientific Publishing Company, Singapore, 2004.
[12] J. Zehnpfennig, G. Bahl, M. Tomes, T. Carmon, Surface optomechanics: calculating optically excited acoustical whispering gallery modes in microspheres, Opt. Express 19 (2011) 14240–14248.
[13] A.H. Choi, Handbook of Optical Microcavities, CRC Press, Boca Raton, FL, 2014.
[14] A.C. Scofield, S.-H. Kim, J.N. Shapiro, A. Lin, B. Liang, A. Scherer, D.L. Huffaker, Bottom-up photonic crystal lasers, Nano Lett. 11 (2011) 5387–5390.
[15] M. Pelton, Modified spontaneous emission in nanophotonic structures, Nat. Photonics 9 (2015) 427–435.
[16] S. Noda, M. Fujita, T. Asano, Spontaneous-emission control by photonic crystals and nanocavities, Nat. Photonics 1 (2007) 449–458.
[17] M.-S. Hwang, J.-H. Choi, K.-Y. Jeong, K.-H. Kim, H.-R. Kim, J.-P. So, H.-C. Lee, J. Kim, S.-H. Kwon, H.-G. Park, Recent advances in nanocavities and their applications, Chem. Commun. 57 (2021) 4875–4885.
[18] J.D. Joannopoulos, R.D. Meade, J.N. Winn, Photonic Crystals : Molding the Flow of Light, second ed., Princeton University Press, Princeton, NJ, 2008.
[19] K.M. Morozov, K.A. Ivanov, A.V. Belonovski, E.I. Girshova, D.d.S. Pereira, C. Menelaou, P. Pander, L.G. Franca, A.P. Monkman, G. Pozina, D.A. Livshits, N. V. Selenin, M.A. Kaliteevski, Efficient UV luminescence from organic-based tamm plasmon structures emitting in the strong-coupling regime, J. Phys. Chem. C 124 (2020) 21656–21663.
[20] D.G. Lidzey, D.D.C. Bradley, A. Armitage, S. Walker, M.S. Skolnick, Photon-Mediated hybridization of frenkel excitons in organic semiconductor microcavities, Science 288 (2000) 1620–1623.
[21] V. Esteso, L. Caliò, H. Espinós, G. Lavarda, T. Torres, J. Feist, F.J. García-Vidal, G. Bottari, H. Míguez, Light-harvesting properties of a subphthalocyanine solar absorber coupled to an optical cavity, Solar RRL 5 (2021) 2100308.
[22] H. Benisty, H.D. Neve, C. Weisbuch, Impact of Planar Microcavity Effects on Light Extraction-Part I: Basic Concepts and Analytical Trends, vol. 34, IEEE J. Quantum Electron, 1998, pp. 1612–1631.
[23] J. Foresi, P.R. Villeneuve, J. Ferrera, E. Thoen, G. Steinmeyer, S. Fan, J. Joannopoulos, L. Kimerling, H.I. Smith, E. Ippen, Photonic-bandgap microcavities in optical waveguides, Nature 390 (1997) 143–145.
[24] Y. Yamamoto, F. Tassone, H. Cao, Semiconductor cavity quantum electrodynamics, springer-verlag Berlin Heidelberg, 2003. Germany.
[25] P. Lalanne, W. Yan, K. Vynck, C. Sauvan, J.-P. Hugonin, Light interaction with photonic and plasmonic resonances, Laser Photon. Rev. 12 (2018) 1700113.
[26] T. Wu, M. Gurioli, P. Lalanne, Nanoscale light confinement: the Q's and V's, ACS, Photonics 8 (2021) 1522–1538.
[27] X. Yu, Y. Yuan, J. Xu, K.-T. Yong, J. Qu, J. Song, Strong coupling in microcavity structures: principle, design, and practical application, Laser Photon. Rev. 13 (2019) 1800219.

[28] R.F. Ribeiro, L.A. Martínez-Martínez, M. Du, J. Campos-Gonzalez-Angulo, J. Yuen-Zhou, Polariton chemistry: controlling molecular dynamics with optical cavities, Chem. Sci. 9 (2018) 6325–6339.

[29] C.W. Wilmsen, H. Temkin, L.A. Coldren, Vertical-cavity Surface-Emitting Lasers: Design, Fabrication, Characterization, and Applications, Cambridge University Press, Cambridge, 2001.

[30] L. Moscardi, G. Lanzani, G.M. Paternò, F. Scotognella, Stimuli-Responsive photonic crystals, Appl. Sci. 11 (2021) 2119.

[31] H. Megahd, C. Oldani, S. Radice, A. Lanfranchi, M. Patrini, P. Lova, D. Comoretto, Aquivion–Poly(N-vinylcarbazole) holistic flory–huggins photonic vapor sensors, Adv. Opt. Mater. 5 (2021) 2002006.

[32] H. Megahd, P. Lova, D. Comoretto, Universal design rules for flory–huggins polymer photonic vapor sensors, Adv. Funct. Mater. 31 (2021) 2009626.

[33] G.M. Paternò, L. Moscardi, S. Donini, D. Ariodanti, I. Kriegel, M. Zani, E. Parisini, F. Scotognella, G. Lanzani, Hybrid one-dimensional plasmonic–photonic crystals for optical detection of bacterial contaminants, J. Phys. Chem. Lett. 10 (2019) 4980–4986.

[34] R. Georgiev, K. Lazarova, M. Vasileva, T. Babeva, All niobia Bragg stacks for optical sensing of vapors, Opt. Quant. Electron. 52 (2020) 114.

[35] S. Normani, N. Dalla Vedova, G. Lanzani, F. Scotognella, G.M. Paternò, Design of 1D photonic crystals for colorimetric and ratiometric refractive index sensing, Opt. Mater. X 8 (2020) 100058.

[36] P. Lova, D. Cortecchia, H.N.S. Krishnamoorthy, P. Giusto, C. Bastianini, A. Bruno, D. Comoretto, C. Soci, Engineering the emission of broadband 2D perovskites by polymer distributed bragg reflectors, ACS Photonics 5 (2018) 867–874.

[37] G.M. Paternò, C. Iseppon, A. D'Altri, C. Fasanotti, G. Merati, M. Randi, A. Desii, E. A.A. Pogna, D. Viola, G. Cerullo, F. Scotognella, I. Kriegel, Solution Processable, Optically Switchable, 1D photonic structures, sci, For. Rep. 8 (2018) 3517–3518.

[38] S.Y. Lim, C.S. Law, M. Markovic, J.K. Kirby, A.D. Abell, A. Santos, Engineering the slow photon effect in photoactive nanoporous anodic alumina gradient-index filters for photocatalysis, ACS Appl. Mater. Interfaces 10 (2018) 24124–24136.

[39] W. Zhang, M. Anaya, G. Lozano, M.E. Calvo, M.B. Johnston, H. Míguez, H. J. Snaith, Highly efficient perovskite solar cells with tunable structural color, Nano Lett. 15 (2015) 1698–1702.

[40] G. Canazza, F. Scotognella, G. Lanzani, S. De Silvestri, M. Zavelani-Rossi, D. Comoretto, Lasing from all-polymer microcavities, Laser Phys. Lett. 11 (2014), 035804.

[41] P. Lalanne, S. Mias, J.P. Hugonin, Two physical mechanisms for boosting the quality factor to cavity volume ratio of photonic crystal microcavities, Opt. Express 12 (2004) 458–467.

[42] N. Nawi, B.Y. Majlis, M.A. Mahdi, R.M. De La Rue, M. Lončar, A.R. Md Zain, Enhancement and reproducibility of high quality factor, one-dimensional photonic crystal/photonic wire (1D PhC/PhW) microcavities, J. Eur. Opt. Soc., Rapid publ. 14 (2018) 6.

[43] S.L. Portalupi, M. Galli, C. Reardon, T.F. Krauss, L. O'Faolain, L.C. Andreani, D. Gerace, Planar photonic crystal cavities with far-field optimization for high coupling efficiency and quality factor, Opt. Express 18 (2010) 16064–16073.

[44] P. Lalanne, J.P. Hugonin, J.M. Gérard, Electromagnetic study of the quality factor of pillar microcavities in the small diameter limit, Appl. Phys. Lett. 84 (2004) 4726–4728.

[45] H. Lohmeyer, K. Sebald, C. Kruse, R. Kröger, J. Gutowski, D. Hommel, J. Wiersig, N. Baer, F. Jahnke, Confined optical modes in monolithic II-VI pillar microcavities, Appl. Phys. Lett. 88 (2006), 051101.

[46] P. Velha, E. Picard, T. Charvolin, E. Hadji, J.C. Rodier, P. Lalanne, D. Peyrade, Ultra-High Q/V Fabry-Perot microcavity on SOI substrate, Opt. Express 15 (2007) 16090–16096.

[47] A. Muller, E.B. Flagg, J.R. Lawall, G.S. Solomon, Ultrahigh-finesse, low-mode-volume Fabry-Perot microcavity, Opt. Lett. 35 (2010) 2293–2295.

[48] D. Comoretto, Organic and Hybrid Photonic Crystals, Springer International Publishing, Basel, 2015.

[49] P. Lova, G. Manfredi, D. Comoretto, Advances in functional solution processed planar one-dimensional photonic crystals, Adv. Opt. Mater. 6 (2018), 1800730–1800726.

[50] Y. Zhang, M. Lončar, Ultra-high quality factor optical resonators based on semiconductor nanowires, Opt. Express 16 (2008) 17400–17409.

[51] S.E. Kushnir, T.Y. Komarova, K.S. Napolskii, High-quality-factor anodic alumina optical microcavities prepared by cyclic anodizing with voltage versus optical path length modulation, J. Mater. Chem. C 8 (2020) 3991–3995.

[52] D. Urbonas, T. Stöferle, F. Scafirimuto, U. Scherf, R.F. Mahrt, Zero-dimensional organic exciton–polaritons in tunable coupled Gaussian defect microcavities at room temperature, ACS Photonics 3 (2016) 1542–1545.

[53] G. Khitrova, H.M. Gibbs, F. Jahnke, M. Kira, S.W. Koch, Nonlinear optics of normal-mode-coupling semiconductor microcavities, Rev. Mod. Phys. 71 (1999) 1591–1639.

[54] C.C. Katsidis, D.I. Siapkas, General transfer-matrix method for optical multilayer systems with coherent, partially coherent, and incoherent interference, Appl. Opt. 41 (2002) 3978–3987.

[55] M. Ściesiek, W. Pacuski, J.-G. Rousset, M. Parlińska-Wojtan, A. Golnik, J. Suffczyński, Design and control of mode interaction in coupled ZnTe optical microcavities, Cryst. Growth Des 17 (2017) 3716–3723.

[56] K. Sawicki, T.J. Sturges, M. Ściesiek, T. Kazimierczuk, K. Sobczak, A. Golnik, W. Pacuski, J. Suffczyński, Polariton lasing and energy-degenerate parametric scattering in non-resonantly driven coupled planar microcavities, Nanophotonics 10 (2021) 2421–2429.

[57] H. Benisty, H.D. Neve, C. Weisbuch, Impact of planar microcavity effects on light extraction-Part II: selected exact simulations and role of photon recycling, IEEE J. Quant. Electron. 34 (1998) 1632–1643.

[58] E.F. Schubert, N.E.J. Hunt, M. Micovic, R.J. Malik, D.L. Sivco, A.Y. Cho, G. J. Zydzik, Highly efficient light-emitting diodes with microcavities, Science 265 (1994) 943–945.

[59] N.E.J. Hunt, E.F. Schubert, R.F. Kopf, D.L. Sivco, A.Y. Cho, G.J. Zydzik, Increased fiber communications bandwidth from a resonant cavity light emitting diode emitting at λ=940 nm, Appl. Phys. Lett. 63 (1993) 2600–2602.

[60] P. Lova, V. Grande, G. Manfredi, M. Patrini, S. Herbst, F. Würthner, D. Comoretto, All-polymer photonic microcavities doped with perylene bisimide j-aggregates, Adv. Opt. Mater. 5 (2017) 1700523.

[61] Y. Li, L.M. Fortes, A. Chiappini, M. Ferrari, R.M. Almeida, High quality factor Er-doped Fabry–Perot microcavities by sol–gel processing, J. Phys. D Appl. Phys. 42 (2009) 205104.

[62] V.G. Golubev, A.A. Dukin, A.V. Medvedev, A.B. Pevtsov, A.V. Sel'kin, N. A. Feoktistov, Fabry-Perot a-Si:H/a-SiOx:H microcavities with an erbium-doped a-Si:H active layer, Semiconductors 35 (2001) 1213–1221.

[63] G. Manfredi, P. Lova, F. Di Stasio, R. Krahne, D. Comoretto, Directional fluorescence spectral narrowing in all-polymer microcavities doped with CdSe/CdS dot-in-rod nanocrystals, ACS Photonics 4 (2017) 1761–1769.

[64] D.G. Gevaux, A.J. Bennett, R.M. Stevenson, A.J. Shields, P. Atkinson, J. Griffiths, D. Anderson, G.A.C. Jones, D.A. Ritchie, Enhancement and suppression of spontaneous emission by temperature tuning InAs quantum dots to photonic crystal cavities, Appl. Phys. Lett. 88 (2006) 131101.

[65] B. Romeira, A. Fiore, Purcell effect in the stimulated and spontaneous emission rates of nanoscale semiconductor lasers, IEEE J. Quant. Electron. 54 (2018) 1–12.

[66] H. Cho, J. Chung, J. Song, J. Lee, H. Lee, J. Lee, J. Moon, S. Yoo, N.S. Cho, Importance of Purcell factor for optimizing structure of organic light-emitting diodes, Opt. Express 27 (2019) 11057–11068.

[67] J. Wang, H. Xu, R. Su, Y. Peng, J. Wu, T.C.H. Liew, Q. Xiong, Spontaneously coherent orbital coupling of counterrotating exciton polaritons in annular perovskite microcavities, Light Sci. Appl. 10 (2021) 45.

[68] X. Zheng, L. Zhang, Photonic nanostructures for solar energy conversion, Energy Environ. Sci. 9 (2016) 2511–2532.

[69] D.G. Lidzey, D.M. Coles, Strong coupling in organic and hybrid-semiconductor microcavity structures, in: D. Comoretto (Ed.), Organic and Hybrid Photonic Crystals, Springer International Publishing, Basel, 2015, pp. 243–273.

[70] K.S. Menghrajani, W.L. Barnes, Strong coupling beyond the light-line, ACS Photonics 7 (2020) 2448–2459.

[71] O. Benson, Assembly of hybrid photonic architectures from nanophotonic constituents, Nature 480 (2011) 193–199.

[72] M.S. Tame, K.R. McEnery, Ş.K. Özdemir, J. Lee, S.A. Maier, M.S. Kim, Quantum plasmonics, Nat. Phys. 9 (2013) 329–340.

[73] M. Hertzog, M. Wang, J. Mony, K. Börjesson, Strong light–matter interactions: a new direction within chemistry, Chem. Soc. Rev. 48 (2019) 937–961.

[74] R. Coccioli, M. Boroditsky, K. Kim, Y. Rahmat-Samii, E. Yablonovitch, Smallest possible electromagnetic mode volume in a dielectric cavity, IEE proc, J Optoelectron 145 (1998) 391–397.

[75] K. Srinivasan, M. Borselli, O. Painter, A. Stintz, S. Krishna, Cavity Q, mode volume, and lasing threshold in small diameter AlGaAs microdisks with embedded quantum dots, Opt. Express 14 (2006) 1094–1105.

[76] J.D. Jackson, Classical Electrodynamics, John Wiley & Sons., New York, 1999.

[77] R.P. Stanley, R. Houdré, U. Oesterle, M. Gailhanou, M. Ilegems, Ultrahigh finesse microcavity with distributed Bragg reflectors, Appl. Phys. Lett. 65 (1994) 1883–1885.

[78] E. Dahal, D. Allemeier, B. Isenhart, K. Cianciulli, M.S. White, Characterization of higher harmonic modes in Fabry–Pérot microcavity organic light emitting diodes, Sci. Rep. 11 (2021) 8456.

[79] P. Lova, H. Megahd, P. Stagnaro, M. Alloisio, M. Patrini, D. Comoretto, Strategies for dielectric contrast enhancement in 1D planar polymeric photonic crystals, Appl. Sci. 10 (2020) 4122.

[80] N. Yogesh, V. Subramanian, Field confinement and quality factor of the multilayer cavity resonators, J. Appl. Phys. 110 (2011) 114519.

[81] T. Rivera, J.-P. Debray, J.M. Gérard, B. Legrand, L. Manin-Ferlazzo, J.L. Oudar, Optical losses in plasma-etched AlGaAs microresonators using reflection spectroscopy, Appl. Phys. Lett. 74 (1999) 911–913.

[82] P. Michler, Single quantum dots: fundamentals, applications and new concepts, Springer-Verlag Berlin Heidelberg, 2003. Germany.

[83] L. Martiradonna, L. Carbone, M.D. Giorgi, L. Manna, G. Gigli, R. Cingolani, M. D. Vittorio, High Q-factor colloidal nanocrystal-based vertical microcavity by hot embossing technology, Appl. Phys. Lett. 88 (2006) 181108.

[84] X. Wu, Y. Wang, Q. Chen, Y.-C. Chen, X. Li, L. Tong, X. Fan, High-Q, low-mode-volume microsphere-integrated Fabry–Perot cavity for optofluidic lasing applications, Photon. Res. 7 (2019) 50–60.

[85] X. Wu, Q. Chen, Y. Wang, X. Tan, X. Fan, Stable high-Q bouncing ball modes inside a fabry–pérot cavity, ACS Photonics 6 (2019) 2470–2478.

[86] F. Li, Y. Li, Y. Cai, P. Li, H. Tang, Y. Zhang, Tunable open-access microcavities for solid-state quantum photonics and polaritonics, Adv. Quantum Technol 2 (2019) 1900060.

[87] M. Aspelmeyer, T.J. Kippenberg, F. Marquardt, Cavity optomechanics, Rev. Mod. Phys. 86 (2014) 1391–1452.

[88] M. Dusel, S. Betzold, S. Brodbeck, S. Herbst, F. Würthner, D. Friedrich, B. Hecht, S. Höfling, C.P. Dietrich, Three-dimensional photonic confinement in imprinted liquid crystalline pillar microcavities, Appl. Phys. Lett. 110 (2017) 201113.

[89] C.P. Dietrich, M. Karl, J. Ohmer, U. Fischer, M.C. Gather, S. Höfling, Molding photonic boxes into fluorescent emitters by direct laser writing, Adv. Mater 29 (2017) 1605236.

[90] M. Guina, A. Rantamäki, A. Härkönen, Optically pumped VECSELs: review of technology and progress, J. Phys. D Appl. Phys. 50 (2017) 383001.

[91] J. Gerard, B. Gayral, Strong Purcell effect for InAs quantum boxes in three-dimensional solid-state microcavities, J. Lightwave Technol. 17 (1999) 2089–2095.

[92] G. Lecamp, J.P. Hugonin, P. Lalanne, R. Braive, S. Varoutsis, S. Laurent, A. Lemaître, I. Sagnes, G. Patriarche, I. Robert-Philip, I. Abram, Submicron-diameter semiconductor pillar microcavities with very high quality factors, Appl. Phys. Lett. 90 (2007), 091120.

[93] W.L. Barnes, G. Björk, J.M. Gérard, P. Jonsson, J.A.E. Wasey, P.T. Worthing, V. Zwiller, Solid-state single photon sources: light collection strategies, Eur, Phys. J. D 18 (2002) 197–210.

[94] S. Reitzenstein, C. Hofmann, A. Gorbunov, M. Strauß, S.H. Kwon, C. Schneider, A. Löffler, S. Höfling, M. Kamp, A. Forchel, AlAs/GaAs micropillar cavities with quality factors exceeding 150.000, Appl. Phys. Lett. 90 (2007) 251109.

[95] N. Chauvin, L. Balet, B. Alloing, C. Zinoni, L. Li, A. Fiore, L. Grenouillet, P. Gilet, N. Olivier, A. Tchelnokov, M. Terrier, J.-M. Gérard, Enhanced spontaneous emission from InAs/GaAs quantum dots in pillar microcavities emitting at telecom wavelengths, Opt. Lett. 32 (2007) 2747–2749.

[96] K. Tanaka, T. Nakamura, W. Takamatsu, M. Yamanishi, Y. Lee, T. Ishihara, Cavity-Induced changes of spontaneous emission lifetime in one-dimensional semiconductor microcavities, Phys. Rev. Lett. 74 (1995) 3380–3383.

[97] K. Sebald, M. Seyfried, S. Klembt, C. Kruse, Optical properties of photonic molecules and elliptical pillars made of ZnSe-based microcavities, Opt. Express 19 (2011) 19422–19429.

[98] M. Bayer, T. Gutbrod, J.P. Reithmaier, A. Forchel, T.L. Reinecke, P.A. Knipp, A. A. Dremin, V.D. Kulakovskii, Optical modes in photonic molecules, Phys. Rev. Lett. 81 (1998) 2582–2585.

[99] M.R. Vázquez, V. Bharadwaj, B. Sotillo, S.-Z.A. Lo, R. Ramponi, N.I. Zheludev, G. Lanzani, S.M. Eaton, C. Soci, Optical NP problem solver on laser-written waveguide platform, Opt. Express 26 (2018) 702–710.

[100] S.S. Guduru, F. Scotognella, A. Chiasera, V. Sreeramulu, L. Criante, K. C. Vishnubhatla, M. Ferrari, R. Ramponi, G. Lanzani, R.M. Vázquez, Highly integrated lab-on-a-chip for fluorescence detection, Opt. Eng. 55 (2016), 097102.

[101] H.-Z. Song, W. Zhang, L.-B. Yu, Z.M. Wang, Micropillar cavity design for 1.55-μm quantum-dot single-photon sources, J. Electron. Sci. Technol 17 (2019) 221–230.

[102] H.-Z. Song, K. Takemoto, T. Miyazawa, M. Takatsu, S. Iwamoto, M. Ekawa, T. Yamamoto, Y. Arakawa, High quality-factor Si/SiO2-InP hybrid micropillar cavities with submicrometer diameter for 1.55-μm telecommunication band, Opt. Express 23 (2015) 16264–16272.

[103] Y. Zhang, M. Lončar, Submicrometer diameter micropillar cavities with high quality factor and ultrasmall mode volume, Opt. Lett. 34 (2009) 902–904.

[104] M. Lermer, N. Gregersen, F. Dunzer, S. Reitzenstein, S. Höfling, J. Mørk, L. Worschech, M. Kamp, A. Forchel, Bloch-wave engineering of quantum dot micropillars for cavity quantum electrodynamics experiments, Phys. Rev. Lett. 108 (2012), 057402.

[105] T. Jakubczyk, H. Franke, T. Smoleński, M. Ściesiek, W. Pacuski, A. Golnik, R. Schmidt-Grund, M. Grundmann, C. Kruse, D. Hommel, P. Kossacki, Inhibition and enhancement of the spontaneous emission of quantum dots in micropillar cavities with radial-distributed bragg reflectors, ACS Nano 8 (2014) 9970–9978.

[106] N. Carlon Zambon, P. St-Jean, M. Milićević, A. Lemaître, A. Harouri, L. Le Gratiet, O. Bleu, D.D. Solnyshkov, G. Malpuech, I. Sagnes, S. Ravets, A. Amo, J. Bloch, Optically controlling the emission chirality of microlasers, Nat. Photonics 13 (2019) 283–288.

[107] M. Bayer, T.L. Reinecke, F. Weidner, A. Larionov, A. McDonald, A. Forchel, Inhibition and enhancement of the spontaneous emission of quantum dots in structured microresonators, Phys. Rev. Lett. 86 (2001) 3168–3171.

[108] M. Galbiati, L. Ferrier, D.D. Solnyshkov, D. Tanese, E. Wertz, A. Amo, M. Abbarchi, P. Senellart, I. Sagnes, A. Lemaître, E. Galopin, G. Malpuech, J. Bloch, Polariton condensation in photonic molecules, Phys. Rev. Lett. 108 (2012) 126403.

[109] K. Liao, X. Hu, T. Gan, Q. Liu, Z. Wu, C. Fan, X. Feng, C. Lu, Y.-c. Liu, Q. Gong, Photonic molecule quantum optics, Adv. Opt. Photon 12 (2020) 60–134.

[110] M. Karl, S. Li, T. Passow, W. Löffler, H. Kalt, M. Hetterich, Localized and delocalized modes in coupled optical micropillar cavities, Opt. Express 15 (2007) 8191–8196.

[111] A. Dikopoltsev, T.H. Harder, E. Lustig, O.A. Egorov, J. Beierlein, A. Wolf, Y. Lumer, M. Emmerling, C. Schneider, S. Höfling, M. Segev, S. Klembt, Topological insulator vertical-cavity laser array, Science 373 (2021) 1514–1517.

[112] N. Sidqi, C. Clark, G.S. Buller, G.K.V.V. Thalluri, J. Mitrofanov, Y. Noblet, Comparative study of dielectric coating materials for micro-cavity applications, Opt. Mater. Express 9 (2019) 3452–3468.

[113] K. Seshan, Handbook of Thin Film Deposition Techniques Principles, Methods, Equipment and Applications, second ed., Noyes Publications, Norwich, NY, 2002.

[114] K. Biermann, E.A. Cerda-Méndez, M. Höricke, P.V. Santos, R. Hey, Controlled growth of exciton–polariton microcavities using in situ spectral reflectivity measurements, J. Cryst. Growth 323 (2011) 56–59.

[115] A. Convertino, A. Capobianchi, A. Valentini, E.N.M. Cirillo, High reflectivity bragg reflectors based on a gold nanoparticle/teflon-like composite material as a new approach to organic solvent detection, Sens, Actuators B 100 (2004) 212–215.

[116] A.M. Adawi, A. Cadby, L.G. Connolly, W.-C. Hung, R. Dean, A. Tahraoui, A. M. Fox, A.G. Cullis, D. Sanvitto, M.S. Skolnick, D.G. Lidzey, Spontaneous emission control in micropillar cavities containing a fluorescent molecular dye, Adv. Mater 18 (2006) 742–747.

[117] L. Persano, A. Camposeo, P.D. Carro, E. Mele, R. Cingolani, D. Pisignano, Very high-quality distributed Bragg reflectors for organic lasing applications by reactive electron-beam deposition, Opt. Express 14 (2006) 1951–1956.

[118] G. Bjork, On the spontaneous lifetime change in an ideal planar microcavity-transition from a mode continuum to quantized modes, IEEE J. Quant. Electron. 30 (1994) 2314–2318.

[119] Q. Xu, C. Piermarocchi, Y.V. Pershin, G.J. Salamo, M. Xiao, X. Wang, C.-K. Shih, Giant up-conversion efficiency of InGaAs quantum dots in a planar microcavity, sci, For. Rep. 4 (2014) 3953.

[120] S. Unsleber, Y.-M. He, S. Gerhardt, S. Maier, C.-Y. Lu, J.-W. Pan, N. Gregersen, M. Kamp, C. Schneider, S. Höfling, Highly indistinguishable on-demand resonance fluorescence photons from a deterministic quantum dot micropillar device with 74% extraction efficiency, Opt. Express 24 (2016) 8539–8546.

[121] T. Jakubczyk, W. Pacuski, T. Smoleński, A. Golnik, M. Florian, F. Jahnke, C. Kruse, D. Hommel, P. Kossacki, Pronounced Purcell enhancement of spontaneous emission in CdTe/ZnTe quantum dots embedded in micropillar cavities, Appl. Phys. Lett. 101 (2012) 132105.

[122] T. Thomay, T. Hanke, M. Tomas, F. Sotier, K. Beha, V. Knittel, M. Kahl, K. M. Whitaker, D.R. Gamelin, A. Leitenstorfer, R. Bratschitsch, Colloidal ZnO quantum dots in ultraviolet pillar microcavities, Opt. Express 16 (2008) 9791–9794.

[123] F.L. Al-Jashaam, R. Jayaprakash, D.M. Coles, A.J. Musser, K. Georgiou, D. G. Lidzey, Optical-mode structure of micropillar microcavities containing a fluorescent conjugated polymer, Adv. Quantum Technol 3 (2020) 1900067.

[124] C. Rupprecht, N. Lundt, M. Wurdack, P. Stepanov, E. Estrecho, M. Richard, E. A. Ostrovskaya, S. Höfling, C. Schneider, Micro-mechanical assembly and characterization of high-quality Fabry–Pérot microcavities for the integration of two-dimensional materials, Appl. Phys. Lett. 118 (2021) 103103.

[125] A. Chiasera, C. Meroni, F. Scotognella, Y.G. Boucher, G. Galzerano, A. Lukowiak, D. Ristic, G. Speranza, S. Valligatla, S. Varas, L. Zur, M. Ivanda, G.C. Righini, S. Taccheo, R. Ramponi, M. Ferrari, Coherent emission from fully Er3+ doped monolithic 1-D dielectric microcavity fabricated by rf-sputtering, Opt. Mater. 87 (2019) 107–111.

[126] A. Alyamani, D. Sanvitto, A.A. Khalifa, M.S. Skolnick, T. Wang, F. Ranalli, P. J. Parbrook, A. Tahraoui, R. Airey, GaN hybrid microcavities in the strong coupling regime grown by metal-organic chemical vapor deposition on sapphire substrates, J. Appl. Phys. 101 (2007), 093110.

[127] J.-R. Chen, T.-C. Lu, Y.-C. Wu, S.-C. Lin, W.-R. Liu, W.-F. Hsieh, C.-C. Kuo, C.-C. Lee, Large vacuum Rabi splitting in ZnO-based hybrid microcavities observed at room temperature, Appl. Phys. Lett. 94 (2009), 061103.

[128] S.F. Chichibu, T. Ohmori, N. Shibata, T. Koyama, Dielectric SiO2/ZrO2 distributed Bragg reflectors for ZnO microcavities prepared by the reactive helicon-wave-excited-plasma sputtering method, Appl. Phys. Lett. 88 (2006) 161914.

[129] J. Shang, C. Cong, Z. Wang, N. Peimyoo, L. Wu, C. Zou, Y. Chen, X.Y. Chin, J. Wang, C. Soci, W. Huang, T. Yu, Room-temperature 2D semiconductor activated vertical-cavity surface-emitting lasers, Nat. Commun. 8 (2017) 543.

[130] N. Dawson, K.D. Singer, J.H. Andrews, M. Crescimanno, G. Mao, J. Petrus, H. Song, E. Baer, Post-process tunability of folded one-dimensional all-polymer photonic crystal microcavity lasers, Nonlin. Opt. Quant. Opt 45 (2012) 101–111.

[131] J.H. Andrews, M. Crescimanno, K.D. Singer, E. Baer, Melt-processed polymer multilayer distributed feedback lasers: Progress and prospects, J. Polym. Sci., Part B: Polym. Phys. 52 (2014) 251–271.

[132] N. Valappil, M. Luberto, V.M. Menon, I. Zeylikovich, T.K. Gayen, J. Franco, B. B. Das, R.R. Alfano, Solution processed microcavity structures with embedded quantum dots, Photonics Nanostruct, Fundam. Appl. 5 (2007) 184–188.

[133] J.-G. Rousset, J. Kobak, E. Janik, M. Parlinska-Wojtan, T. Slupinski, A. Golnik, P. Kossacki, M. Nawrocki, W. Pacuski, Distributed Bragg reflectors obtained by combining Se and Te compounds: influence on the luminescence from CdTe quantum dots, J. Appl. Phys. 119 (2016) 183105.

[134] S. Gehrsitz, F.K. Reinhart, C. Gourgon, N. Herres, A. Vonlanthen, H. Sigg, The refractive index of AlxGa1−xAs below the band gap: accurate determination and empirical modeling,, J. Appl. Phys. 87 (2000) 7825–7837.

[135] J. Piprek, Semiconductor Optoelectronic Devices: Introduction to Physics and Simulation, Academic Press, Cambridge, MA, 2003.

[136] K. Sawicki, J.-G. Rousset, R. Rudniewski, W. Pacuski, M. Ściesiek, T. Kazimierczuk, K. Sobczak, J. Borysiuk, M. Nawrocki, J. Suffczyński, Triple threshold lasing from a photonic trap in a Te/Se-based optical microcavity, Commun. Phys. 2 (2019) 38.

[137] C. Meroni, F. Scotognella, Y. Boucher, A. Lukowiak, D. Ristic, G. Speranza, S. Varas, L. Zur, M. Ivanda, S. Taccheo, R. Ramponi, G.C. Righini, M. Ferrari, A. Chiasera, Low-threshold coherent emission at 1.5 μm from fully Er3+ doped monolithic 1D dielectric microcavity fabricated using radio frequency sputtering, Ceramics 2 (2019) 74–85.

[138] V. Robbiano, G.M. Paternò, A.A. La Mattina, S.G. Motti, G. Lanzani, F. Scotognella, G. Barillaro, Room-temperature low-threshold lasing from monolithically integrated nanostructured porous silicon hybrid microcavities, ACS Nano 12 (2018) 4536–4544.

[139] Z. Chen, V. Robbiano, G.M. Paternò, G. Carnicella, A. Debrassi, A.A. La Mattina, S. Mariani, A. Minotto, G. Egri, L. Dähne, F. Cacialli, G. Barillaro, Nanoscale photoluminescence manipulation in monolithic porous silicon oxide microcavity coated with rhodamine-labeled polyelectrolyte via electrostatic nanoassembling, Adv. Opt. Mater. 9 (2021) 2100036.

[140] A.M. Vredenberg, N.E.J. Hunt, E.F. Schubert, D.C. Jacobson, J.M. Poate, G. J. Zydzik, Controlled atomic spontaneous emission from Er3+ in a transparent Si/SiO_2 microcavity, Phys. Rev. Lett. 71 (1993) 517–520.

[141] S. Dirr, S. Wiese, H.H. Johannes, D. Ammermann, A. Böhler, W. Grahn, W. Kowalsky, Luminescence enhancement in microcavity organic multilayer structures, Synth. Met. 91 (1997) 53–56.

[142] L. Persano, P.D. Carro, E. Mele, R. Cingolani, D. Pisignano, M. Zavelani-Rossi, S. Longhi, G. Lanzani, Monolithic polymer microcavity lasers with on-top evaporated dielectric mirrors, Appl. Phys. Lett. 88 (2006) 121110.

[143] S. Tokito, T. Tsutsui, Y. Taga, Microcavity organic light-emitting diodes for strongly directed pure red, green, and blue emissions, J. Appl. Phys. 86 (1999) 2407–2411.

[144] C.B. Poitras, M. Lipson, H. Du, M.A. Hahn, T.D. Krauss, Photoluminescence enhancement of colloidal quantum dots embedded in a monolithic microcavity, Appl. Phys. Lett. 82 (2003) 4032–4034.

[145] M. Wang, J. Lin, Y.-C. Hsiao, X. Liu, B. Hu, Investigating underlying mechanism in spectral narrowing phenomenon induced by microcavity in organic light emitting diodes, Nat. Commun. 10 (2019) 1614.

[146] H. Yokoyama, Physics, Device Applications, Of optical microcavities, Science 256 (1992) 66–70.

[147] D. Goldberg, V.M. Menon, Enhanced amplified spontaneous emission from colloidal quantum dots in all-dielectric monolithic microcavities, Appl. Phys. Lett. 102 (2013), 081119.

[148] S. Robert, H. Rigneault, F. Lamarque, Spontaneous emission properties of Pr ions located in planar dielectric microcavities, J. Opt. Soc. Am. B 15 (1998) 1773–1779.

[149] H. Rigneault, S. Monneret, Modal analysis of spontaneous emission in a planar microcavity, Phys. Rev. A 54 (1996) 2356–2368.

[150] M. Wei, S.K. Rajendran, H. Ohadi, L. Tropf, M.C. Gather, G.A. Turnbull, I.D. W. Samuel, Low-threshold polariton lasing in a highly disordered conjugated polymer, Optica 6 (2019) 1124–1129.

[151] S.K. Rajendran, M. Wei, H. Ohadi, A. Ruseckas, G.A. Turnbull, I.D.W. Samuel, Low threshold polariton lasing from a solution-processed organic semiconductor in a planar microcavity, Adv. Opt. Mater. 7 (2019) 1801791.

[152] R. Jayaprakash, K. Georgiou, H. Coulthard, A. Askitopoulos, S.K. Rajendran, D. M. Coles, A.J. Musser, J. Clark, I.D.W. Samuel, G.A. Turnbull, P.G. Lagoudakis, D. G. Lidzey, A hybrid organic–inorganic polariton LED,, Light Sci. Appl. 8 (2019) 81.

[153] D.P. Puzzo, M.G. Helander, P.G. O'Brien, Z. Wang, N. Soheilnia, N. Kherani, Z. Lu, G.A. Ozin, Organic light-emitting diode microcavities from transparent conducting metal oxide photonic crystals, Nano Lett. 11 (2011) 1457–1462.

[154] G.M. Paternò, L. Moscardi, I. Kriegel, F. Scotognella, G. Lanzani, Electro-Optic, Magneto-Optic Photonic, Devices based on multilayer photonic structures, SPIE Proc. 8 (2018) 1–8.

[155] L. Xiao, Y. Lv, J. Lin, Y. Hu, W. Dong, X. Guo, Y. Fan, N. Zhang, J. Zhao, Y. Wang, X. Liu, WO3-Based electrochromic distributed bragg reflector: toward electrically tunable microcavity luminescent device, Adv. Opt. Mater. 6 (2018) 1700791.

[156] D.J. Norris, Y.A. Vlasov, Chemical approaches to three-dimensional semiconductor photonic crystals, Adv. Mater 13 (2001) 371–376.

[157] S. Chénais, S. Forget, Recent advances in solid-state organic lasers, Polym. Int. 61 (2012) 390–406.

[158] P. Lova, P. Giusto, F.D. Stasio, G. Manfredi, G.M. Paternò, D. Cortecchia, C. Soci, D. Comoretto, All-polymer methylammonium lead iodide perovskite microcavity, Nanoscale 11 (2019) 8978–8983.

[159] W. Gaëtan, F. Rolando, S. Stefan, Z. Libero, Nanoporous films with low refractive index for large-surface broad-band anti-reflection coatings, Macromol. Chem. Phys. 295 (2010) 628–636.

[160] M.K. Ghosh, K.L. Mittal, Polyimides Fundamentals and Applications, first ed., CRC Press, LLC Boca Raton, FL, 1996.

[161] T. Higashihara, M. Ueda, Recent progress in high refractive index polymers, Macromolecules 48 (2015) 1915–1929.

[162] R.A. Dine-Hart, W.W. Wright, A study of some properties of aromatic imides,, Makromol. Chem. 143 (1971) 189–206.

[163] J.G. Liu, Y. Nakamura, Y. Suzuki, Y. Shibasaki, S. Ando, M. Ueda, Highly Refractive, Transparent Polyimides, Derived from 4,4'-[m-Sulfonylbis (phenylenesulfanyl)]diphthalic anhydride and various sulfur-containing aromatic diamines, Macromolecules 40 (2007) 7902–7909.

[164] R.A. Minns, R.A. Gaudiana, Design and synthesis of high refractive index polymers, II, J. Macromol. Sci. A 29 (1992) 19–30.

[165] M.A. Olshavsky, H.R. Allcock, Polyphosphazenes with high refractive indices: synthesis, characterization, and optical properties, Macromolecules 28 (1995) 6188–6197.

[166] M. Olshavsky, H.R. Allcock, Polyphosphazenes with high refractive Indices: optical dispersion and molar refractivity, Macromolecules 30 (1997) 4179–4183.

[167] T. Fushimi, H.R. Allcock, Cyclotriphosphazenes with sulfur-containing side groups: refractive index and optical dispersion, Dalton Trans. (2009) 2477–2481.

[168] W. Qiang, Z. Xingjie, Q. Xianping, Ö. Gözde, S. Karin, K. Anton, V. Brigitte, High refractive index hyperbranched polymers prepared by two naphthalene-bearing monomers via thiol-yne reaction, Macromol. Chem. Phys. 217 (2016) 1977–1984.

[169] Q. Wei, R. Pötzsch, X. Liu, H. Komber, A. Kiriy, B. Voit, P.-A. Will, S. Lenk, S. Reineke, Hyperbranched polymers with high transparency and inherent high refractive index for application in organic light-emitting diodes, Adv. Funct. Mater. 26 (2016) 2545–2553.

[170] N.G. Ireni, R. Narayan, P. Basak, K.V.S. Raju, Functional polyurethane–urea coatings from sulfur rich hyperbranched polymers and an evaluation of their anticorrosion and optical properties, New J. Chem. 40 (2016) 8081–8092.

[171] W. Groh, A. Zimmermann, What is the lowest refractive index of an organic polymer? Macromolecules 24 (1991) 6660–6663.

[172] S.V. Radice, P. Srinivasan, D. Comoretto, S. Gazzo, One-dimensional planar photonic crystals including fluoropolymer compositions and corresponding fabrication methods, in: I.A.P.U.T.P.C.T. (PCT), 2016.

[173] J.Q. Xi, M.F. Schubert, J.K. Kim, E.F. Schubert, M. Chen, S.-Y. Lin, W. Liu, J. A. Smart, Optical thin-film materials with low refractive index for broadband elimination of Fresnel reflection, Nat. Photonics 1 (2007) 176–179.

[174] R.J. Gher, R.W. Boyd, Optical properties of nanostructured optical materials, Chem. Mater. 8 (1996) 1807.

[175] C.-C. Liu, J.-G. Li, S.-W. Kuo, Co-templates method provides hierarchical mesoporous silicas with exceptionally ultra-low refractive indices, RSC Adv. 4 (2014) 20262–20272.

[176] J.R.C. Smirnov, M. Ito, M.E. Calvo, C. López-López, A. Jiménez-Solano, J. F. Galisteo-López, P. Zavala-Rivera, K. Tanaka, E. Sivaniah, H. Míguez, Adaptable ultraviolet reflecting polymeric multilayer coatings of high refractive index contrast, Adv. Opt. Mater. 3 (2015) 1633–1639.

[177] P. Giusto, P. Lova, G. Manfredi, S. Gazzo, B. Srinivasan, S.V. Radice, D. Comoretto, Colorimetric Detection of Perfluorinated Compounds by All-Polymer Photonic Transducers ACS Omega 3, 2018, pp. 7517–7522.

[178] S.V. Radice, P. Gavezotti, G. Simeone, M. Albano, G. Canazza, S. Congiu, Photonic crystals, S.S.P.I. S.P.A., 2014.

[179] S. Bachevillier, H.-K. Yuan, A. Strang, A. Levitsky, G.L. Frey, A. Hafner, D.D. C. Bradley, P.N. Stavrinou, N. Stingelin, Fully solution-processed photonic structures from inorganic/organic molecular hybrid materials and commodity polymers, Adv. Funct. Mater. 29 (2019) 1808152.

[180] M. Russo, M. Campoy-Quiles, P. Lacharmoise, T.A.M. Ferenczi, M. Garriga, W. R. Caseri, N. Stingelin, One-pot synthesis of polymer/inorganic hybrids: toward readily accessible, low-loss, and highly tunable refractive index materials and patterns, J. Polym. Sci., Part B: Polym. Phys. 50 (2012) 65–74.

[181] F. Scotognella, A. Monguzzi, F. Meinardi, R. Tubino, DFB laser action in a flexible fully plastic multilayer, Phys. Chem. Chem. Phys. 12 (2009) 337–340.

[182] G. Manfredi, P. Lova, F. Di Stasio, P. Rastogi, R. Krahne, D. Comoretto, Lasing from dot-in-rod nanocrystals in planar polymer microcavities, RSC Adv. 8 (2018) 13026–13033.

[183] M. Athanasiou, P. Papagiorgis, A. Manoli, C. Bernasconi, M.I. Bodnarchuk, M. V. Kovalenko, G. Itskos, Efficient amplified spontaneous emission from solution-processed CsPbBr3 nanocrystal microcavities under continuous wave excitation, ACS Photonics 8 (2021) 2120–2129.

[184] R.E. Fern, A. Onton, Refractive index of AlAs, J. Appl. Phys. 42 (1971) 3499–3500.

[185] A.D. Rakić, M.L. Majewski, Modeling the optical dielectric function of GaAs and AlAs: extension of Adachi's model, J. Appl. Phys. 80 (1996) 5909–5914.

[186] D.E. Aspnes, S.M. Kelso, R.A. Logan, R. Bhat, Optical properties of AlxGa1−x as, J. Appl. Phys. 60 (1986) 754–767.

[187] M.J. Weber, CRC Handbook of Laser Science and Technology Supplement 2: Optical Materials, CRC press, Boca Raton, FL, 2003.

[188] T. Amotchkina, M. Trubetskov, D. Hahner, V. Pervak, Characterization of e-beam evaporated Ge, YbF3, ZnS, and LaF3 thin films for laser-oriented coatings, Appl. Opt. 59 (2020) A40–A47.

[189] S. Ozaki, S. Adachi, Optical constants of cubic ZnS, Jpn. J. Appl. Phys. 32 (1993) 5008–5013.

[190] K. Sato, S. Adachi, Optical properties of ZnTe, J. Appl. Phys. 73 (1993) 926–931.

[191] D.T.F. Marple, Refractive index of ZnSe, ZnTe, and CdTe, J. Appl. Phys. 35 (1964) 539–542.

[192] S. Adachi, T. Taguchi, Optical properties of ZnSe, Phys. Rev. B 43 (1991) 9569–9577.

[193] L.V. Rodríguez-de Marcos, J.I. Larruquert, J.A. Méndez, J.A. Aznárez, Self-consistent optical constants of SiO2 and Ta2O5 films, Opt. Mater. Express 6 (2016) 3622–3637.

[194] M.R. Vogt, Development of Physical Models for the Simulation of Optical Properties of Solar Cell Modules, Gottfried Wilhelm Leibniz Universität, Hannover, 2015.

[195] K. Luke, Y. Okawachi, M.R.E. Lamont, A.L. Gaeta, M. Lipson, Broadband mid-infrared frequency comb generation in a Si3N4 microresonator, Opt. Lett. 40 (2015) 4823–4826.

[196] S. Sarkar, V. Gupta, M. Kumar, J. Schubert, P.T. Probst, J. Joseph, T.A.F. König, Hybridized guided-mode resonances via colloidal plasmonic self-assembled grating, ACS Appl. Mater. Interfaces 11 (2019) 13752–13760.

[197] T.J. Bright, J.I. Watjen, Z.M. Zhang, C. Muratore, A.A. Voevodin, D.I. Koukis, D. B. Tanner, D.J. Arenas, Infrared optical properties of amorphous and nanocrystalline Ta2O5 thin films, J. Appl. Phys. 114 (2013), 083515.

[198] L. Gao, F. Lemarchand, M. Lequime, Exploitation of multiple incidences spectrometric measurements for thin film reverse engineering, Opt. Express 20 (2012) 15734–15751.

[199] N. Uchida, Optical properties of single-crystal Paratelluri$teTeO_2$, Phys. Rev. B 4 (1971) 3736–3745.

[200] D.L. Wood, K. Nassau, Refractive index of cubic zirconia stabilized with yttria, Appl. Opt. 21 (1982) 2978–2981.

[201] I.H. Malitson, A redetermination of some optical properties of calcium fluoride,, Appl. Opt. 2 (1963) 1103–1107.

[202] H.H. Li, Refractive index of alkali halides and its wavelength and temperature derivatives, J. Phys. Chem. Ref. Data 5 (1976) 329–528.

[203] M.F. Al-Kuhaili, Optical properties of hafnium oxide thin films and their application in energy-efficient windows, Opt. Mater. 27 (2004) 383–387.

[204] X. Zhang, J. Qiu, X. Li, J. Zhao, L. Liu, Complex refractive indices measurements of polymers in visible and near-infrared bands, Appl. Opt. 59 (2020) 2337–2344.
[205] L. Fornasari, F. Floris, M. Patrini, D. Comoretto, F. Marabelli, Demonstration of fluorescence enhancement via Bloch surface waves in all-polymer multilayer structures, Phys. Chem. Chem. Phys. 18 (2016) 14086–14093.
[206] M.F. Schubert, J.-Q. Xi, J.K. Kim, E.F. Schubert, Distributed Bragg reflector consisting of high- and low-refractive-index thin film layers made of the same material, Appl. Phys. Lett. 90 (2007) 141115.
[207] E. Afsharipour, B. Park, C. Shafai, Determination of reactive RF-sputtering parameters for fabrication of SiOx films with specified refractive index, for highly reflective SiOx distributed bragg reflector, IEEE Photonics J 9 (2017) 1–16.
[208] V.M. Menon, M. Luberto, N.V. Valappil, S. Chatterjee, Lasing from InGaP quantum dots in a spin-coated flexible microcavity, Opt. Express 16 (2008) 19535–19540.
[209] M. Kahl, T. Thomay, V. Kohnle, K. Beha, J. Merlein, M. Hagner, A. Halm, J. Ziegler, T. Nann, Y. Fedutik, U. Woggon, M. Artemyev, F. Pérez-Willard, A. Leitenstorfer, R. Bratschitsch, Colloidal quantum dots in all-dielectric high-Q pillar microcavities, Nano Lett. 7 (2007) 2897–2900.
[210] B.Y. Jung, N.Y. Kim, C. Lee, C.K. Hwangbo, C. Seoul, Control of resonant wavelength from organic light-emitting materials by use of a Fabry-Perot microcavity structure, Appl. Opt. 41 (2002) 3312–3318.
[211] P.J. Harding, T.G. Euser, Y.-R. Nowicki-Bringuier, J.-M. Gérard, W.L. Vos, Dynamical ultrafast all-optical switching of planar GaAs/AlAs photonic microcavities, Appl. Phys. Lett. 91 (2007) 111103.
[212] J. Vučković, M. Pelton, A. Scherer, Y. Yamamoto, Optimization of three-dimensional micropost microcavities for cavity quantum electrodynamics, Phys. Rev. A 66 (2002), 023808.
[213] T. Kitada, T. Kanbara, K. Morita, T. Isu, A GaAs/AlAs multilayer cavity with self-assembled InAs quantum dots embedded in strain-relaxed barriers for ultrafast all-optical switching applications,, Appl. Phys. Express 1 (2008), 092302.
[214] P. Lova, G. Manfredi, L. Boarino, M. Laus, G. Urbinati, T. Losco, F. Marabelli, V. Caratto, M. Ferretti, M. Castellano, C. Soci, D. Comoretto, Hybrid ZnO: polystyrene nanocomposite for all-polymer photonic crystals, phys, Status Solidi C 12 (2015) 158–162.
[215] R.J. Nussbaumer, W.R. Caseri, P. Smith, T. Tervoort, Polymer-TiO_2 nanocomposites: a route towards visually transparent broadband uv filters and high refractive index materials,, Macromol. Chem. Phys. 288 (2003) 44–49.
[216] T. Ogata, R. Yagi, N. Nakamura, Y. Kuwahara, S. Kurihara, Modulation of polymer refractive indices with diamond nanoparticles for metal-free multilayer film mirrors, ACS Appl. Mater. Interfaces 4 (2012) 3769–3772.
[217] H. Althues, J. Henle, S. Kaskel, Functional inorganic nanofillers for transparent polymers, Chem. Soc. Rev. 36 (2007) 1454–1465.
[218] N. Suzuki, Y. Tomita, K. Ohmori, M. Hidaka, K. Chikama, Highly transparent ZrO2 nanoparticle-dispersed acrylate photopolymers for volume holographic recording, Opt. Express 14 (2006) 12712–12719.
[219] F. Papadimitrakopoulos, P. Wisniecki, D.E. Bhagwagar, Mechanically attrited silicon for high refractive index nanocomposites, Chem. Mater 9 (1997) 2928–2933.
[220] C. Lü, Z. Cui, Z. Li, B. Yang, J. Shen, High refractive index thin films of ZnS/polythiourethane nanocomposites, J. Mater. Chem. 13 (2003) 526–530.
[221] J.-g. Liu, Y. Nakamura, T. Ogura, Y. Shibasaki, S. Ando, M. Ueda, Optically transparent sulfur-containing Polyimide−TiO2 nanocomposite films with high refractive index and negative pattern formation from poly(amic acid)−TiO2 nanocomposite film, Chem. Mater 20 (2008) 273–281.
[222] G.M. Paternò, L. Moscardi, S. Donini, A.M. Ross, S.M. Pietralunga, N. Dalla Vedova, S. Normani, I. Kriegel, G. Lanzani, F. Scotognella, Integration of bio-responsive silver in 1D photonic crystals: towards the colorimetric detection of bacteria, Faraday Discuss 223 (2020) 125–135.
[223] C. Paquet, P.W. Cyr, E. Kumacheva, I. Manners, Polyferrocenes: metallopolymers with tunable and high refractive indices, Chem. Commun. (J. Chem. Soc. Sect. D) (2004) 234–235.
[224] M. Häußler, J.W.Y. Lam, A. Qin, K.K.C. Tse, M.K.S. Li, J. Liu, C.K.W. Jim, P. Gao, B.Z. Tang, Metallized hyperbranched polydiyne: a photonic material with a large refractive index tunability and a spin-coatable catalyst for facile fabrication of carbon nanotubes, Chem. Commun. (J. Chem. Soc. Sect. D) (2007) 2584–2586.
[225] S.D. Bhagat, J. Chatterjee, B. Chen, A.E. Stiegman, High refractive index polymers based on thiol–ene cross-linking using polarizable inorganic/organic monomers, Macromolecules 45 (2012) 1174–1181.
[226] M. Castellano, A. Turturro, E. Marsano, L. Conzatti, S. Vicini, Hydrophobation of silica surface by silylation with new organo-silanes bearing a polybutadiene oligomer tail, Polym. Compos. 35 (2014) 1603–1613.
[227] G. Boccalero, C. Jean-Mistral, M. Castellano, C. Boragno, Soft, hyper-elastic and highly-stable silicone-organo-clay dielectric elastomer for energy harvesting and actuation applications, Composites, Part B 146 (2018) 13–19.
[228] C. Jansen, F. Neubauer, J. Helbig, D.M. Mittleman, M. Koch, Flexible Bragg reflectors for the terahertz regime composed of polymeric compounds, in: 2007 Joint 32nd International Conference on Infrared and Millimeter Waves and the 15th International Conference on Terahertz Electronics, 2007, pp. 984–986.
[229] T. Uehara, M. Nakagawa, O. Sugihara, Preparation of UV-cured organic–inorganic hybrid materials with low refractive index for multilayer film applications, Opt. Mater. Express 3 (2013) 1351–1357.
[230] T. Druffel, N. Mandzy, M. Sunkara, E. Grulke, Polymer nanocomposite thin film mirror for the infrared region, Small 4 (2008) 459–461.
[231] P. Lova, G. Manfredi, L. Boarino, A. Comite, M. Laus, M. Patrini, F. Marabelli, C. Soci, D. Comoretto, Polymer distributed bragg reflectors for vapor sensing, ACS Photonics 2 (2015) 537–543.
[232] P. Lova, Selective polymer distributed bragg reflector vapor sensors, Polymers 10 (2018) 1161.
[233] S.J. Jeon, M.C. Chiappelli, R.C. Hayward, Photocrosslinkable nanocomposite multilayers for responsive 1D photonic crystals, Adv. Funct. Mater. 26 (2016) 722–728.
[234] A. Convertino, A. Capobianchi, A. Valentini, E.N.M. Cirillo, A new approach to organic solvent detection: high-reflectivity bragg reflectors based on a gold nanoparticle/teflon-like composite material, Adv. Mater 15 (2003) 1103–1105.
[235] J.d. Pino, J. Feist, F.J. Garcia-Vidal, Quantum theory of collective strong coupling of molecular vibrations with a microcavity mode, New J. Phys. 17 (2015), 053040.
[236] N. Tessler, G.J. Denton, R.H. Friend, Lasing from conjugated-polymer microcavities, Nature 382 (1996) 695–697.
[237] R.T. Grant, P. Michetti, A.J. Musser, P. Gregoire, T. Virgili, E. Vella, M. Cavazzini, K. Georgiou, F. Galeotti, C. Clark, J. Clark, C. Silva, D.G. Lidzey, Efficient radiative pumping of polaritons in a strongly coupled microcavity by a fluorescent molecular dye, Adv. Opt. Mater. 4 (2016) 1615–1623.
[238] R.M. Almeida, S. Portal, Photonic band gap structures by sol–gel processing, Curr. Opin. Solid State Mater. Sci. 7 (2003) 151–157.
[239] E.D. Martínez, A. Prado, M. González, S. Anguiano, L. Tosi, L.S. Alarcón, H. Pastoriza, Integrating photoluminescent nanomaterials with photonic nanostructures, J. Lumin. 233 (2021) 117870.
[240] T. Tawara, H. Gotoh, T. Akasaka, N. Kobayashi, T. Saitoh, Cavity polaritons in InGaN microcavities at room temperature, Phys. Rev. Lett. 92 (2004) 256402.
[241] C. Weisbuch, M. Nishioka, A. Ishikawa, Y. Arakawa, Observation of the coupled exciton-photon mode splitting in a semiconductor quantum microcavity, Phys. Rev. Lett. 69 (1992) 3314–3317.
[242] H. Jeon, J. Ding, W. Patterson, A.V. Nurmikko, W. Xie, D.C. Grillo, M. Kobayashi, R.L. Gunshor, Blue-green injection laser diodes in (Zn,Cd)Se/ZnSe quantum wells, Appl. Phys. Lett. 59 (1991) 3619–3621.
[243] G. Panzarini, L.C. Andreani, A. Armitage, D. Baxter, M.S. Skolnick, V.N. Astratov, J.S. Roberts, A.V. Kavokin, M.R. Vladimirova, M.A. Kaliteevski, Exciton-light coupling in single and coupled semiconductor microcavities: polariton dispersion and polarization splitting, Phys. Rev. B 59 (1999) 5082–5089.
[244] D.G. Deppe, D.L. Huffaker, Quantum Well, Quantum Dot, Light emitters confined in oxide-semiconductor microcavities, Opt. Photon. News 9 (1998) 30.
[245] M. Kira, F. Jahnke, S.W. Koch, J.D. Berger, D.V. Wick, T.R. Nelson, G. Khitrova, H. M. Gibbs, Quantum theory of nonlinear semiconductor microcavity luminescence explaining "boser" experiments, Phys. Rev. Lett. 79 (1997) 5170–5173.
[246] G. Ramon, U. Mizrahi, N. Akopian, S. Braitbart, D. Gershoni, T.L. Reinecke, B. D. Gerardot, P.M. Petroff, Emission characteristics of quantum dots in planar microcavities, Phys. Rev. B 73 (2006) 205330.
[247] M. Sasani Ghamsari, Chip-Scale Quantum Emitters, Quantum Rep, vol. 3, 2021, pp. 615–642.
[248] A.J. Shields, Semiconductor quantum light sources, Nat. Photonics 1 (2007) 215–223.
[249] Q. Zhang, R. Su, W. Du, X. Liu, L. Zhao, S.T. Ha, Q. Xiong, Advances in small perovskite-based lasers, Small Methods 1 (2017) 1700163.
[250] J. Wang, R. Cao, P. Da, Y. Wang, T. Hu, L. Wu, J. Lu, X. Shen, F. Xu, G. Zheng, Z. Chen, Purcell effect in an organic-inorganic halide perovskite semiconductor microcavity system, Appl. Phys. Lett. 108 (2016), 022103.
[251] A. Brehier, R. Parashkov, J.S. Lauret, E. Deleporte, Strong exciton-photon coupling in a microcavity containing layered perovskite semiconductors, Appl. Phys. Lett. 89 (2006) 171110.
[252] L. Reeves, Y. Wang, T.F. Krauss, 2D material microcavity light emitters: to lase or not to lase? Adv. Opt. Mater. 6 (2018) 1800272.
[253] J.K. Day, M.-H. Chung, Y.-H. Lee, V.M. Menon, Microcavity enhanced second harmonic generation in 2D MoS2, Opt. Mater. Express 6 (2016) 2360–2365.
[254] E. Janitz, M.K. Bhaskar, L. Childress, Cavity quantum electrodynamics with color centers in diamond, Optica 7 (2020) 1232–1252.
[255] A. Reiserer, G. Rempe, Cavity-based quantum networks with single atoms and optical photons, Rev. Mod. Phys. 87 (2015) 1379–1418.
[256] D.G. Lidzey, D.D.C. Bradley, T. Virgili, A. Armitage, M.S. Skolnick, S. Walker, Room temperature polariton emission from strongly coupled organic semiconductor microcavities, Phys. Rev. Lett. 82 (1999) 3316–3319.
[257] D.M. Coles, N. Somaschi, P. Michetti, C. Clark, P.G. Lagoudakis, P.G. Savvidis, D. G. Lidzey, Polariton-mediated energy transfer between organic dyes in a strongly coupled optical microcavity, Nat. Mater. 13 (2014) 712–719.
[258] D.G. Lidzey, D.D.C. Bradley, M.S. Skolnick, T. Virgili, S. Walker, D.M. Whittaker, Strong exciton–photon coupling in an organic semiconductor microcavity, Nature 395 (1998) 53–55.
[259] K. Pradeesh, J.J. Baumberg, G.V. Prakash, Strong exciton-photon coupling in inorganic-organic multiple quantum wells embedded low-Q microcavity, Opt. Express 17 (2009) 22171–22178.
[260] J. Keeling, S. Kéna-Cohen, Bose–einstein condensation of exciton-polaritons in organic microcavities, Annu. Rev. Phys. Chem. 71 (2020) 435–459.
[261] M. Wei, A. Ruseckas, V.T.N. Mai, A. Shukla, I. Allison, S.-C. Lo, E.B. Namdas, G. A. Turnbull, I.D.W. Samuel, Low threshold room temperature polariton lasing from fluorene-based oligomers, Laser Photon. Rev. 15 (2021) 2100028.
[262] L. Berthelot, J. Tardy, A. Gagnaire, J. Joseph, B. Masenelli, M. Garrigues, V. H. Tran, H. Rigneault, Modified spontaneous emission in oligo (p-phenylene vinylene) planar microcavities, Opt. Mater. 9 (1998) 25–33.